University of Massachusetts Amherst

ScholarWorks@UMass Amherst

Doctoral Dissertations

Dissertations and Theses

October 2018

QUANTUM PHASE TRANSITIONS IN DISORDERED BOSON SYSTEMS

Zhiyuan Yao
University of Massachusetts Amherst

Follow this and additional works at: https://scholarworks.umass.edu/dissertations_2

Part of the Atomic, Molecular and Optical Physics Commons, Condensed Matter Physics Commons, and the Quantum Physics Commons

QUANTUM PHASE TRANSITIONS IN DISORDERED BOSON SYSTEMS

A Dissertation Presented

by

ZHIYUAN YAO

Submitted to the Graduate School of the
University of Massachusetts Amherst in partial fulfillment
of the requirements for the degree of

DOCTOR OF PHILOSOPHY

September 2018

Department of Physics

QUANTUM PHASE TRANSITIONS IN DISORDERED BOSON SYSTEMS

A Dissertation Presented

by

ZHIYUAN YAO

Approved as to style and content by:

_____

Nikolay V. Prokof'ev, Chair

_____

Boris V. Svistunov, Member

_____

Tigran Sedrakyan, Member

_____

Murugappan Muthukumar, Member

_____

Narayanan Menon, Department Chair
Department of Physics

ACKNOWLEDGMENTS

and for their love. There are many more people to whom I am grateful, and I want to take this opportunity to thank them all.

ABSTRACT

QUANTUM PHASE TRANSITIONS IN DISORDERED BOSON SYSTEMS

SEPTEMBER 2018

ZHIYUAN YAO

B.Sc., UNIVERSITY OF SCIENCE AND TECHNOLOGY OF CHINA

Ph.D., UNIVERSITY OF MASSACHUSETTS AMHERST

Directed by: Professor Nikolay V. Prokof'ev and Professor Boris V. Svistunov

In this dissertation, we study the superfluid-insulator quantum phase transition in disordered boson systems. Recently, there has been considerable controversy over the validity of the scaling relation, $\phi = \nu z = \nu d$ with ϕ the critical-temperature exponent, ν the correlation length exponent, z the dynamical critical exponent, and d the spatial dimension, of the superfluid–Bose-glass quantum phase transition in three dimensions. Experiments and numerical simulations on disordered quantum magnets reported $\phi \approx 1.1(1)$ and $\nu \approx 0.75(10)$, contradicting the scaling relation and the associated conventional scaling hypothesis for the singular part of the free energy [4,5]. We determine various critical exponents of the superfluid–Bose-glass quantum phase transition in three-dimensional disordered Bose-Hubbard model through extensive Monte Carlo simulations. Our numerical study shows the previous studies on disordered quantum magnets were performed outside the quantum critical region, and our results for the critical exponents are in perfect agreement with $\phi = \nu z = \nu d$.

We next move to study theoretically and numerically the superfluid-insulator quantum phase transition in one-dimensional disordered boson systems. While the superfluid-insulator transition in the weak disorder limit is well understood through the perturbative renormalization group study by Giamarchi and Schulz, transitions in the strong disorder regime are beyond the reach of this method. This problem was recently attacked by Altman *et al.* with the real space renormalization group method. They reached the conclusion that the superfluid-insulator transition in the strong disorder regime can be explained by the Coulomb blockade physics of weak links. However, their method is actually uncontrolled. Taking account of the crucial role of the hydrodynamic renormalization of weak links, finally, Pollet *et al.* put forward an asymptotically exact renormalization group theory of the superfluid-insulator transition. Based on this theory, we are able to provide an accurate description of the interplay between the well-known Giamarchi-Schulz criticality and the new weak-link criticality. A significant part of the ground-state phase diagram of one-dimensional disordered Bose-Hubbard model at unit filling is also determined numerically. In particular, we established the position of the multicritical point beyond which the new weak-link criticality takes over of the Giamarchi–Schulz criticality.

TABLE OF CONTENTS

LIST OF FIGURES

LIST OF SYMBOLS

$\hbar$	reduced Planck constant which is set to be 1 in our system of units
k_B	Boltzmann constant which is set to be 1 in our system of units
β	inverse temperature $\beta = (k_B T)^{-1}$
d	spatial dimension
V	system volume or external potential
Z	partition function $Z = \mathrm{Tr} e^{-\beta H}$ or $Z = \mathrm{Tr} e^{-\beta(H-\mu N)}$
χ	susceptibility
κ	compressibility $\kappa = \partial n / \partial \mu$
g	tuning parameter of a quantum phase transition with g_c the critical value
t	hopping amplitude
U	on-site interaction strength or potential part of the Hamiltonian
μ	chemical potential
$\delta\mu_i$	on-site disordered potential
Ω	characteristic energy scale near the quantum phase transition
Δ	strength of on-site potential disorder
δ	reduced control parameter for a quantum phase transition $\delta = |g - g_c|/g_c$
f_s	singular part of free energy density
ξ	correlation length
ξ_τ	correlation length in imaginary time direction
ν	correlation length critical exponent
z	dynamical critical exponent
ϕ	critical-temperature exponent or phase of a Luttinger liquid
η	critical exponent for anomalous dimension
W	winding number
Λ_{s}	superfluid stiffness related to superfluid mass density by $\rho_s = (\frac{m}{\hbar})^2 \Lambda_{\mathrm{s}}$
u	phonon velocity of a Luttinger liquid
K	Luttinger liquid parameter $K = \pi\sqrt{\kappa\Lambda_{\mathrm{s}}}$, kinetic part of the Hamiltonian, or coupling parameter of the J-current model
J	strength of a weak link
$J_{n,\alpha}$	integer valued bond variable of the J-current model
ζ	microscopic parameter characterizing the scaling of the bare strength of the typical weakest link with increasing system size, $J_0^{(L)} \propto 1/L^{1-\zeta}$

LIST OF ABBREVIATIONS

1D	one-dimensional
2D	two-dimensional
QPT	quantum phase transition
QCP	quantum critical point
FSS	finite-size scaling
BH	Bose-Hubbard
DBH	disordered Bose-Hubbard
GS	Giamarchi-Schulz
SF	superfluid
MI	Mott insulator
BG	Bose glass
NL	normal liquid
SF-BG	superfluid–Bose-glass
SF-I	superfluid-insulator
RG	renormalization group
KT	Kosterlitz–Thouless
BKT	Berezinskii–Kosterlitz–Thouless
LL	Luttinger liquid
sXY	scratched-XY

INTRODUCTION

The interplay between interaction and disorder has been a fascinating yet extremely difficult subject in quantum physics. For fermion systems, the effect of disorder can be explored alone without invoking the complications brought about by interactions. For boson systems, however, interaction has to be included from the beginning since the ground state for the non-interacting boson system is pathological with all the bosons condensing into the lowest potential well. To keep the local density and the compressibility of the system finite, interaction has to be included in a fundamental way, and we have to solve the whole problem with both interaction and disorder all at once.

As shown by Giamarchi and Schulz using perturbative renormalization group (RG) method [40, 41], in one dimension, disorder can drive a superfluid-insulator (SF-I) quantum phase transition (QPT) in the weak disorder regime. The critical condition for this transition turns out to be universal with $K_c = 3/2$ where K is the Luttinger liquid (LL) parameter related to the compressibility, κ, and the superfluid stiffness, Λ_s, by $K = \pi\sqrt{\kappa\Lambda_s}$. Following the pioneering work of Giamarchi and Schulz, the general problem of the combined effect of interaction and disorder in boson systems in arbitrary dimension was systematically investigated by Fisher *et al.* [7]. In particular, they studied the ground-state properties of the disordered Bose-Hubbard (DBH) model with generic diagonal disorder. While in the pure case (no disorder), the phase transition is between a superfluid (SF) and a Mott-insulator (MI), a new insulating phase—the Bose-glass (BG) phase—will emerge in the presence of disorder. They also argued that the BG phase is expected to always intervene between the SF and the MI phases [subsequently this was proved to be a theorem in Refs. [15, 16]],

i.e., there is no direct SF-MI transition in the presence of disorder. The dynamical critical exponent of the superfluid–Bose-glass (SF-BG) transition was shown to be always equal to the spatial dimension, $z = d$, and the critical-temperature exponent, ϕ, governing the scaling behavior of critical temperature of the superfluid–normal-liquid (SF-NL) classical phase transition near the quantum critical point, $T_c \propto |g_c - g|^\phi$, was predicted to obey the scaling relation, $\phi = \nu z$.

However, recent experiments and quantum Monte Carlo simulations on Br-doped DTN, a disordered $S = 1$ antiferromagnet, reported $\phi = 1.1(1)$ and $\nu = 0.75(10)$ [4,5] for the SF-BG quantum phase transition (QPT) in three dimensions, in direct contradiction with an exact bound for QPTs in disordered systems, $\nu \geq 2/d$ [14], and the exact relation $\phi = \nu z = \nu d$. As a result, the conventional scaling hypothesis for the singular part of free energy of the SF-BG transition was challenged. We investigated this problem by Monte Carlo simulations and found the reported $\phi = 1.1(1)$ was actually fitted in regions outside of the quantum critical region. After adopting another strategy with broader quantum critical region, our extensive classical and quantum Monte Carlo simulations validate the scaling relation $\phi = \nu z$ with $z = d = 3$, $\phi = 2.7(2)$, and $\nu = 0.88(5)$.

In one dimension, there have been considerable efforts and progress in uncovering the combined effect of interaction and disorder after pioneering work of Giamarchi and Schulz (GS). For a single impurity, no matter how weak or strong, Kane and Fisher reached the remarkable conclusion that the single impurity will drive a pure LL to an insulator whenever $K < 1$, and that the system remains LL if $K > 1$ [43, 44]. Later, it was recognized that both the Giamarchi–Schulz physics and the Kane-Fisher physics can be easily understood by evoking Popov's hydrodynamic action in terms of the phase field [47]. In this representation, superfluidity is exclusively destroyed by instanton–anti-instanton pairs, or, equivalently, by vortex–anti-vortex pairs in the (1+1)-dimensional phase field, suggesting $K_c = 3/2$ was the only critical condition for SF-I transition in generic disordered systems. However, inspired by

the special roles of weak links (strong potential barriers) in destroying superfluidity classically in one dimension, in a series of papers, Altman *et al.* studied the SF-I transition in one-dimensional (1D) disordered Josephson-junction array with real-space RG method, and found superfluidity can be destroyed by weak links connecting regions of superfluids in the strong disorder regime [51–53, 55]. However, their real-space RG method is not asymptotically exact and is uncontrolled. On the other hand, numerical simulations on the 1D disordered quantum rotor model have found that the critical LL parameter of the SF-I transition indeed becomes non-universal when the disorder strength is above a certain threshold [59], calling for a new theory of SF-I transitions in one dimension.

After a careful study of the effect of weak links, Pollet *et al.* developed an asymptotically exact RG theory of SF-I transition in one-dimensional disordered systems and found weak links are indeed responsible for a new universality class, the weak link criticality, in the strong disorder regime [57]. The critical LL parameter for the weak-link criticality is given by the relation $K_c = \zeta^{-1}$ where ζ^{-1} is a microscopic parameter governing the scaling of the strength of the typical weakest link with increasing system size. Based on this theory, we studied the crossover behavior between the Giamarchi–Schulz criticality and the weak-link criticality, and obtained an analytic description of the crossover behavior [58]. We also applied the theory to study the ground-state phase diagram of the one-dimensional DBH model at unit filling (commensurability is not relevant for the critical behavior of the SF-BG transition [64]) and showed the new weak-link criticality constitutes, roughly speaking, half of the SF-BG critical line.

This thesis is organized as follows. In Chapter 1, we briefly discuss the ground-state phase diagram of the DBH model and the scaling relations of the critical exponents. The path-integral representation, the Worm algorithm, and the J-current model used in our Monte Carlo simulations are introduced in Chapter 2. Our numerical study on the critical

exponents of the SF-BG QPT in three dimensions is presented in Chapter 3. Chapter 4 is devoted to our analytical and numeric studies on SF-I transitions in one dimension.

CHAPTER 1

CRITICAL BEHAVIOR OF DISORDERED BOSON SYSTEMS

1.1   Quantum phase transitions

A quantum phase transition (QPT) is the phase transition of a quantum system at zero temperature where the nature of the ground-state wave function undergoes a qualitative change across the quantum critical point (QCP) [2, 3]. This change can be due to either an actual level-crossing of the ground state and the lowest excited state, or an avoided level-crossing which becomes progressively sharp with increasing system size and results in a singularity in the thermodynamic limit. In either case, the ground-state energy is singular (non-analytic) at the QCP. QPTs caused by actual level crossing are often first order and quantum zero-point fluctuations are not important. On the other hand, QPTs resulted from avoided level-crossings are often continuous phase transitions where fluctuations play a crucial role in determining the critical behavior. Since the latter ones are more common and interesting, we will focus exclusively on the continuous quantum phase transitions from now on. In contrast to classical phase transitions, which are entirely driven by thermal fluctuations, quantum phase transitions are driven only by zero-point fluctuations as a result of Heisenberg's uncertainty principle.

A classical phase transition can be tuned by changing temperature, but a QPT is realized only by tuning certain parameter, g, of the Hamiltonian (the tuning parameter can be chemical potential μ in $H - \mu N$ for the grand canonical ensemble) since $T \equiv 0$ for QPTs by definition. However, QPTs are very similar to classical phase transitions in many respects. In path-integral formulation, a d-dimensional quantum system can often be mapped to a

$(d + 1)$-dimensional classical system with imaginary time being the extra dimension, and g playing essentially the same role as temperature in a classical phase transition. Similar to the correlation length, ξ, in spatial directions, a temporal correlation length, ξ_τ, can be defined in the imaginary time direction.

This becomes evident when one considers the large imaginary time behavior of the following zero-temperature correlation function in Matsubara representation (the space dependence of the operators is suppressed),

$$\langle A(\tau)B(0)\rangle = \sum_n \langle 0\,|A|\,n\rangle\langle n\,|B|\,0\rangle e^{-\tau E_{n0}} \xrightarrow{\tau \to \infty} C\,e^{-\tau\,\Omega}\,, \tag{1.1}$$

where C is a relatively smooth function of τ and Ω is the characteristic energy dictating the asymptotic decay of the correlation function. For a gapped system of which the low-energy spectrum is discrete, the dominant contribution comes from the lowest excited state $|1\rangle$. In this case, $C = \langle 0\,|A|\,1\rangle\langle 1\,|B|\,0\rangle$ and $\Omega = E_{10}$, *i.e.*, the characteristic energy is just the excitation gap. If the system is gapless, the formal sum over the eigenstates becomes an integral, and Ω will be the characteristic energy scale of the low-energy spectral density of the system. In either case, Ω^{-1} can be identified as the correlation length ($\hbar = 1$) in imaginary time direction. Similarly to classical phase transitions, as $g \to g_c$, both ξ and ξ_τ diverge. And the divergences of ξ on both sides of the QCP are captured by a single critical exponent ν. The same is true for ξ_τ. However, since the action for the $(d+1)$-dimensional classical representation is in general anisotropic, it is necessary to introduce a new exponent, the *dynamical critical exponent* z, to characterize the singular behavior of ξ_τ near the QCP,

$$\xi_\tau = \Omega^{-1} \sim \xi^z \sim |g - g_c|^{-\nu z} \tag{1.2}$$

where ν is the conventional *correlation length critical exponent* (from now on we will take ξ and ξ_τ as dimensionless numbers which are scaled with lattice spacing in spatial and

imaginary time directions respectively.). Other critical exponents can be defined similarly. For example, the anomalous exponent η can be defined by the power law behavior of the following correlation function

$$\mathcal{G}(\mathbf{r}, \tau) = \left\langle \hat{\psi}(\mathbf{r}, \tau)\hat{\psi}^\dagger(0,0) \right\rangle - \left\langle \hat{\psi}(\tau) \right\rangle\left\langle \hat{\psi}^\dagger(0) \right\rangle \sim \frac{1}{r^{d+z-2+\eta}} \, g(r/\xi, \tau/\xi_\tau) \qquad (1.3)$$

for long distance and large time near the QCP.
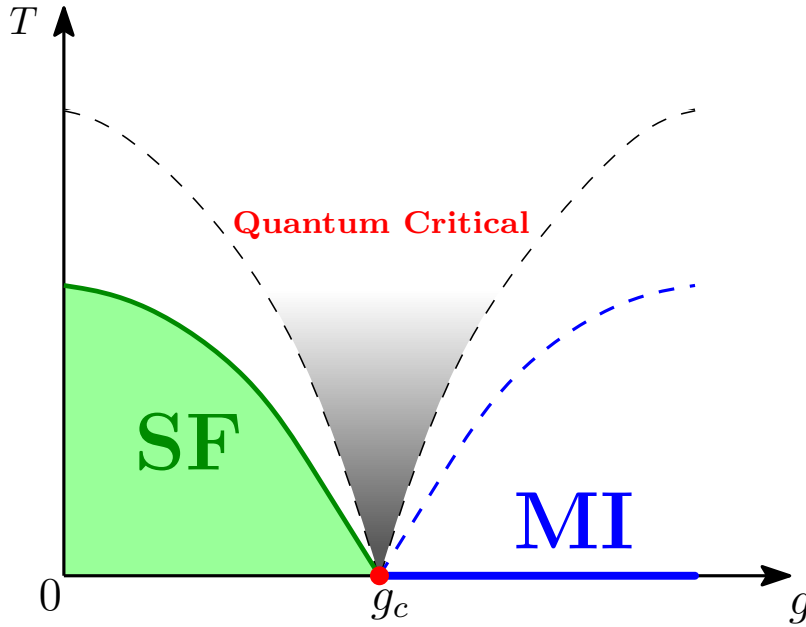
Figure 1.1: A sketch of the finite temperature phase diagram of the pure Bose-Hubbard model in dimensions $d \geq 2$ at integer particle number fillings. The QPT is between a superfluid shown as the green region and a Mott insulator shown as the blue line on the $T = 0$ axis (Mott insulators only exist at zero temperature). At finite temperature, the quantum critical point (the red dot) is at the end of a continuous phase transition line between a superfluid and a normal liquid (right of the green line and above zero temperature). It turns out that the shape of this transition line near the quantum critical point is determined by properties of the QPT at zero temperature. The blue dotted line is not a real phase transition line but a crossover line across which the behavior of the finite temperature conductivity changes quantitatively. The quantum critical region illustrated as the gray shaded region is distinguished from other regions by dynamics [2].

Brute force study of QPTs numerically is also often impractical since simulations are typically performed for finite system sizes at finite temperatures (finite lengths in imaginary time). However, QPTs can still be studied by methods such as finite size scaling (FSS). For example, near the QCP, a scale-invariant physical quantity O such as the winding number (to be discussed in Chapter 2) will take the following scaling form,

$$O(L, \beta) = f(\xi/L, \xi_\tau/L_\tau) = \tilde{f}(L^{1/\nu}\delta, L^z/L_\tau) , \qquad (1.4)$$

where L is the system size, $L_\tau = \hbar\beta$, and $\delta = |g - g_c|/g_c$ is the reduced "temperature" of the $(d+1)$-dimensional classical system. If we fix the value of L^z/L_τ, then for big enough L and $\delta = 0$, the quantity $O(L, \beta)$ will be a constant for different system sizes. This method, in principle, allows us to determine exponents ν and z simultaneously.

Studying QPTs can also help us understand low temperature physics of the system. It is quite common that the quantum critical point is joined by a finite temperature continuous phase line as shown in Fig. 1.1. Because points on the finite temperature phase transition line have to be singularities in physical quantities such as $O(L, \beta)$, *i.e.*, f is singular when ξ_τ/L_τ is equal to a certain constant A, the finite temperature phase transition line is determined by

$$k_B T_c = A \Omega \sim |g_c - g|^{\nu z} , \qquad (1.5)$$

where T_c is the critical temperature of the classical phase transition.

1.2 Ground-state phase diagram of the disordered Bose-Hubbard model

The Hamiltonian of the DBH model is

$$H = -\sum_{<ij>} t_{ij}(b_i^\dagger b_j + \text{H.c.}) + \sum_i \frac{U_i}{2} n_i(n_i - 1) - \sum_i (\mu + \delta\mu_i)n_i \qquad (1.6)$$

8

where <> denotes the summation over nearest-neighbor sites, b_i $(b_i^\dagger)$ is the boson annihilation (creation) operator, $n_i = b_i^\dagger b_i$ is the density operator, t_{ij} is the hopping amplitude, U_i is the on-site repulsion, μ is the chemical potential, and $\delta\mu_i$ is the bounded, disordered on-site potential. Arguably, this is the simplest model that describes the combined effects of interaction and disorder in boson systems. Moreover, this model is also relevant for many experimental systems, such as ^{4}He in porous media (for example Vycor) and on various substrates, disordered Josephson junctions where U_i and t_{ij} depend on the size of the superconducting grains and distances between them, cold atoms in disordered optical lattices [8–10], and disordered quantum magnets [11].

We will focus on the case of diagonal disorder here where both the hopping amplitude and on-site repulsion are site-independent, $t_{ij} = t$ and $U_i = U$, and disorder is only in the on-site potential $\delta\mu_i$. Typically and in the following discussions, $\delta\mu_i$ is taken to be distributed uniformly in $[-\Delta, \Delta]$ and uncorrelated in space, where Δ is the strength of the disorder. The Hamiltonian of the DBH model we will study in this thesis is

$$H = -t \sum_{\langle ij \rangle} (b_i^\dagger b_j + \text{H.c.}) + \frac{U}{2} \sum_i n_i(n_i - 1) - \sum_i (\mu + \delta\mu_i) n_i \,. \tag{1.7}$$

Without randomness, $\Delta = 0$, the model is known as the Bose-Hubbard (BH) model. The ground-state phase diagram of the BH model consists of two phases: a Mott insulator (MI) phase characterized by integer particle number filling, $\langle n_i \rangle = n$, and a gap in particle or hole excitation; and a superfluid phase featuring off-diagonal long range order in dimensions $d \geq 2$ and algebraic quasi-long-range order in one dimension. The properties of the MI phase are easy to understand by considering the limiting case of vanishing hopping, $t = 0$. The Hamiltonian then becomes a sum of on-site Hamiltonians H_i where

$$H_i = \frac{U}{2} n_i(n_i - 1) - \mu n_i \,, \tag{1.8}$$

and it is exactly solvable. The ground-state wave function of the system is a direct product of the ground-state wave function for each site, $|\Psi_0\rangle = \prod_i \otimes |n\rangle_i$. This integer filling remains unchanged in the region $(n-1)U < \mu < nU$ ($n = 0$ if $\mu < 0$) until the degenerate points where $\mu = mU$ (m is a non-negative integer) are reached. The single particle (hole) excitation energy of the system is given by $E_p = nU - \mu$ [$E_h = \mu - (n-1)U$]. Now consider the case of small hopping amplitude $t/U \ll 1$, the ground state will remain an eigenstate of the total particle number operator, $N = \sum_i n_i$, because $[N, H] = 0$ and there is a finite gap for particle or hole excitation. Assuming translational invariance, we immediately reach the conclusion of integer filling per site of the MI.

Clearly, the MI-SF transition is determined by the vanishing of particle or hole excitation of the system. Because the kinetic energy gained by one extra particle (hole) hopping around the system grows with increasing hopping amplitude t, the region of MI will shrink with increasing t, resulting in a lobe shape of the MI phase as illustrated in Fig. 1.2. For the simple reason that $[N, H] = 0$, the particle (hole) excitation energy of the MI phase is given by the distance to the upper (lower) phase boundary along the direction of the chemical potential axis, $E_{10} = |\mu - \mu_c|$ where μ_c is the chemical potential at the transition point. It follows that the value of νz, which controls the singular behavior of the lowest excitation energy E_{10} (E_p or E_h) near the QCP for generic density-driven SF-MI transition away from the tip of the Mott phase, is equal to one, $E_{10} = |\mu - \mu_c| = |\mu - \mu_c|^{\nu z}$, a result valid in arbitrary dimension. The SF-MI transition at the Mott tip with fixed density is different as the first excitation energy E_{10} is the sum of the particle and hole excitation energies, $E_{10} = E_p + E_h$. By introducing an auxiliary field that decouples the hopping term of the Hamiltonian and integrating out the original coherent field, one will arrive at a $(d+1)$-dimensional field theory that features emergent particle-hole symmetry and space-time isotropy at the critical

point [2,7]. Therefore, the universality class of this fixed-density transition is the same as the $(d+1)$-XY universality class, and $z = 1$ because of space-time isotropy. The value, $\nu z = \nu$, determines the singular shape of the SF-MI transition line near the Mott tip. For $d \geq 3$, the shape is parabolic since $\nu = 1/2$.

(a) The ground-state phase diagram of the pure BH model comprises the commensurate MI phase and the SF phase, as illustrated in the figure.

(b) The schematic ground-state phase diagram of the DBH model for relatively weak disorder, $\Delta < U/2$, where the emerging BG phase always intervenes between the MI and SF phase.
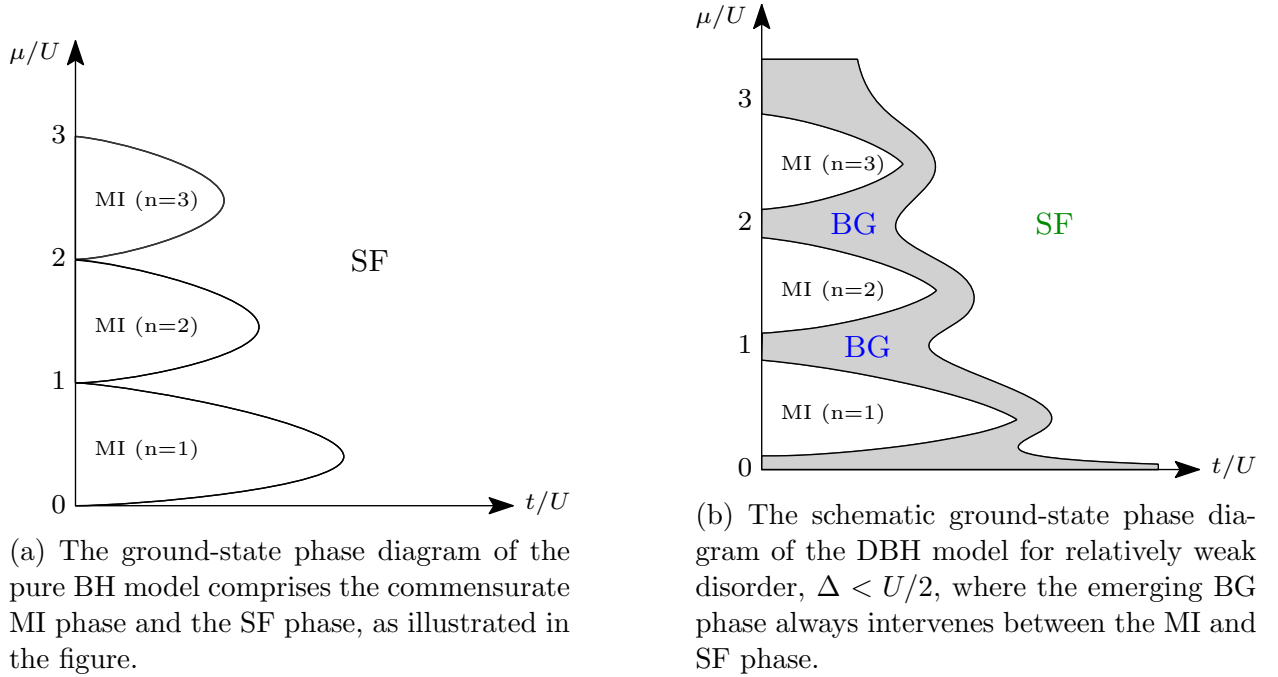
Figure 1.2: A sketch of the ground-state phase diagram of the pure and disordered Bose-Hubbard model.

To understand the QPTs in the DBH model, it is still easier to start with the special case of zero hopping. For a site with integer filling n, the particle and hole excitation energies are given by $nU - \mu - \delta\mu_i$ and $\mu + \delta\mu_i - (n-1)U$ respectively. Because of the randomness in $\delta\mu_i$, the system is only gapped (remains MI) for $(n-1)U + \Delta < \mu < nU - \Delta$ (MI is destroyed whenever $\Delta > U/2$). The density of the system in the gapless region $nU - \Delta < \mu < nU + \Delta$ grows linearly from n to $n+1$ with increasing chemical potential, resulting in a finite and constant compressibility $\kappa = 1/2\Delta$ in this region. This phase is known as the Bose-glass

phase. With nonzero hopping term, for reasons discussed before, the MI region will shrink, and the low energy excitations of the system will be quasi-particle and quasi-hole excitations. The phase boundary between the MI and BG phases can be determined by the rare region considerations. The probability of seeding an arbitrary large region where the chemical potential is shifted upwards or downwards uniformly by Δ is small but finite. These rare regions, if not for their finite sizes, correspond to the phase in the pure case where the chemical potential is μ_r ($\mu + \Delta$ or $\mu - \Delta$). If the phase is superfluid for μ_r in the pure system, these rare regions will be superfluids locally with lowest excitation energies inversely proportional to their volume. Since the size of the rare regions can be arbitrary large in the thermodynamic limit, the system is gapless and not a gapped MI. Actually, it has been proved that the MI-BG phase is determined by the condition $\Delta = E_{g/2} = \min(E_p, E_h)$, $i.e.$, the disorder strength equals the smaller value of the particle and hole excitation energies in the pure system [16]. As a result, the MI-BG phase transition line has a kink at the Mott tip as shown in Fig. 1.2b [17, 18]. The MI-BG transition driven by rare regions depends only on the disorder strength and is of Griffiths-type [19, 20]. Since the probability of seeding a large rare region is exponentially small [21], the Griffiths-McCoy singularity of the BG phase will show up as an essential singularity.

The low energy excitations of the BG phase just outside the MI phase can be viewed as quasi-particles and quasi-holes of the rare regions (SF lakes) on the background of a MI. These excitations are localized for reasons similar to the Anderson localization. Alway from the MI-BG transition line towards the BG-SF transition line, the SF lakes grow in number and size. However, global phase coherence between them is not maintained. This means if we apply a phase twist at the boundary of the system, the phase twist will be absorbed by MI regions. And the free energy of the system remains the same, $i.e.$, the superfluid stiffness Λ_s of the BG phase is zero. While the BG is an insulator, its compressibility is finite. A rough estimate of the compressibility of the BG phase can be given by considering

superfluid lakes with typical size r and separation $R(r)$ [1]. The quasi-particle excitation energy of the SF lake, $E_{N+1} - E_N$, scales with r as $1/\kappa_0(r)r^d$ where $\kappa_0(r)$ is the compressibility of the superfluid lake. Only those superfluid lakes with the quasi-particle (quasi-particle) excitation level in the vicinity of the chemical potential will make a nonzero contribution to the compressibility. Because of the uniform distribution of the on-site disordered chemical potential, the probability of the on-site chemical potential to be in a region $\delta\mu$ near the quasi-particle excitation energy is expected to be $\delta\mu/(E_{N+1} - E_N)$. The compressibility of the system is therefore

$$\kappa = \frac{\partial n}{\partial \mu} \approx \sum_r \lim_{\delta\mu \to 0} \left(\frac{1}{R^d(r)} \frac{\delta\mu}{E_{N+1} - E_N} \right) / \delta\mu \sim \sum_r \kappa_0(r) \frac{r^d}{R^d(r)}. \tag{1.9}$$

A consequence of the finite compressibility (finite density of states of quasi-particle excitations at zero energy) of the BG phase is the infinite uniform superfluid susceptibility χ [7] defined as

$$\chi = \left. \frac{\delta\langle\psi(\boldsymbol{r},\tau)\rangle}{\delta h} \right|_{h=0} = \int_0^{\beta\hbar}\!\!\int d\tau\, d\boldsymbol{r}\, \langle\psi(\boldsymbol{r},\tau)\psi^*(0,0)\rangle = \int_0^{\beta\hbar}\!\!\int d\tau\, d\boldsymbol{r}\, \mathcal{G}(\boldsymbol{r},\tau) \tag{1.10}$$

where the average is calculated for the action

$$S[\psi] = S_0[\psi] + \int_0^{\beta\hbar}\!\!\int d\tau\, d\boldsymbol{r}\, [h\psi^*(\boldsymbol{r},\tau) + h^*\psi(\boldsymbol{r},\tau)] \tag{1.11}$$

with $S_0[\psi]$ the action of the unperturbed system. Since quasi-particle is localized in space, a finite density of states of quasi-particle excitations at zero energy implies a nonzero single-particle density of states $\rho_1(0)$ defined as

$$\rho_1(\omega) = \frac{1}{Z} \sum_n \left| \langle n | \psi^\dagger(r) | 0 \rangle \right|^2 \delta(\omega - \omega_{n0}). \tag{1.12}$$

The large imaginary time behavior of $\mathcal{G}(\boldsymbol{r}, \tau)$ is therefore

$$\mathcal{G}(\boldsymbol{r}, \tau) = \int_0^\infty d\omega \rho_1(\omega) e^{-\omega\tau} \to \rho_1(0)/\tau \,. \tag{1.13}$$

It is evident from Eq. (1.10) that long-range correlation in imaginary time leads to infinite uniform superfluid susceptibility just as the case for the paramagnetic phase of one-dimensional random transverse field Ising model [22].

The size and number of the superfluid lakes grow with increasing hopping amplitude. At certain point, global phase coherence is achieved across the system, and a phase twist at the boundary of the system will result in an increase in free energy. This defines the BG-SF transition point. We have argued that immediately outside the MI phase, the extra small amount of quasi-particles and quasi-holes will be localized, *i.e.*, the BG phase should intervene between the MI and SF phases in the presence of disorder. The absence of a direct MI-SF transition in the presence of disorder was first proved in one dimension based on the RG method [46] and was later proved in general by *theorem of inclusions* which states the transition to the SF phase is always from a gapless phase [1, 15]. The proof follows from the observation that one can always find arbitrary large regions of SF lakes in the BG phase for generic BG-SF transitions which does not depend on the bound of disorder alone (in contrast to the MI-BG transition).

1.3 Scaling relations between critical exponents

The scaling behavior of various physical quantities near the BG-SF quantum critical point can be derived in analogy with the classical continuous phase transition. To this end, we first define the free energy density f of the system as

$$f = \lim_{\beta, V \to \infty} \frac{-1}{\beta V} \ln Z \,. \tag{1.14}$$

14

On approach to the QCP, the system can be viewed as an ensemble of $\beta V / \xi^d \xi_\tau$ independent regions. If we split f into singular part, f_s, and analytic part, f_a, according to hyperscaling in general valid for short-range interactions below the *upper critical dimension* [24, 25], the singular part of the free energy per correlation volume $\xi^d \xi_\tau$ is a finite number A,

$$f_s\, \xi^d \xi_\tau = A\,. \tag{1.15}$$

Furthermore, two-scale-factor universality (hyperuniversality) states that A is universal [26–28].

In terms of $\delta = |g - g_c|/g_c$, the reduced tuning parameter, f_s is expected to behave as

$$f_s(\delta) \sim \delta^{\nu(d+z)} \tag{1.16}$$

on approach to the critical point. Subsequently, the singular behavior of various physical quantities can be determined by performing derivatives with respect to f_s. However, the scaling relation for the superfluid stiffness Λ_s can not be obtained in this way since Λ_s is determined by the response of the system subject to twisted boundary conditions instead of external fields. Noticing that the response to the boundary condition is a finite size effect, the scaling relation for Λ_s can be derived by FSS [7, 23]. For large but finite system size and inverse temperature, f_s can be written as

$$f_s(\delta) \sim \delta^{\nu(d+z)} Y_0\left(\frac{\xi}{L}, \frac{\xi_\tau}{\beta}\right). \tag{1.17}$$

In the presence of phase twist θ along a certain spatial direction, the corresponding singular part of free energy, $f_s^\theta(\delta)$, is

$$f_s^\theta(\delta) \sim \delta^{\nu(d+z)} Y_\theta\left(\frac{\xi}{L}, \frac{\xi_\tau}{\beta}\right). \tag{1.18}$$

15

Here the function Y_0 and Y_θ are of the order of unity functions when $\xi/L \ll 1$ and $\xi_\tau/\beta \ll 1$ since f_s (with and without phase twist) has to reduce to $f_s \sim \delta^{\nu(d+z)}$ for infinite system at zero temperature. Moreover, $Y_0(0, \xi_\tau/\beta) = Y_\theta(0, \xi_\tau/\beta)$ which reflects the fact that the response to phase twist is a finite size effect. Therefore, for large L one would expect $Y_\theta - Y_0 \propto (\xi/L)^2$ in accordance with the definition of a nonzero superfluid stiffness, $f^\theta(\delta) - f(\delta) \propto \Lambda_s L^{-2}$, (the difference of full free energy density equals the difference of singular part of free energy density because the dependence of Y on L, ξ/L, is singular). Equating the difference of free energy calculated in two ways,

$$\Lambda_s \frac{1}{L^2} \sim \delta^{\nu(d+z)} \frac{\xi^2}{L^2} , \tag{1.19}$$

immediately leads to the generalized *Josephson scaling relation*,

$$\Lambda_s \sim \delta^{\nu(d+z-2)} . \tag{1.20}$$

The scaling relation for the full compressibility κ can also be obtained in this way as κ is related to the phase twist along the imaginary time direction. The long-wavelength, low-energy physics of a superfluid is described by the Popov's hydrodynamic action [1],

$$S[\phi] = \int d\boldsymbol{r} \int_0^{\beta\hbar} d\tau \left[in_0(x)\partial_\tau\phi + \frac{\Lambda_s}{2}(\nabla\phi)^2 + \frac{\kappa}{2}(\hbar\partial_\tau\phi)^2 \right] . \tag{1.21}$$

Here $n_0(x)$ (no τ dependence) is the expectation value of the local density, and $\phi(x, \tau)$ is the coarse-grained superfluid phase field. The free energy increase under phase twist along the imaginary time direction, therefore, scales as $f^\theta(\delta) - f(\delta) \propto \beta^{-2}$, and κ scales as

$$\kappa \sim \delta^{\nu(d+z-2z)} = \delta^{\nu(d-z)} . \tag{1.22}$$

Note the "extended-scaling" assumption is made in the derivation of the scaling relations of Λ_s and κ. Strictly speaking, δ is L dependent, and under certain circumstances, the

generalized Josephson scaling relation will get modified [23]. Since κ is finite both in the BG and SF phases, κ should also be finite at the QCP. As a result, the dynamical critical exponent equals the spatial dimension of the system, $z = d$.

At finite temperature, while the insulating BG phase ceases to exist and becomes the normal liquid (NL) phase, the SF phase can persist in dimensions higher than one. In this case, there will be a SF-NL classical phase transition at low temperature (λ transition of ^{4}He is an example). The singular dependence of critical temperature on tunning parameter of the SF-NL transition at low temperature defines the critical-temperature exponent ϕ,

$$T_c(\delta) \sim \delta^\phi \,. \tag{1.23}$$

As shown in Eq. (1.5), ϕ is given by $\phi = \nu z$.

For transitions in pure systems, the introduction of weak disorder, such as weak on-site or bond disorder, can destabilize the fixed point. Consequently, the sharp phase transition in the pure system is rounded (no phase transition anymore), or a new disorder fixed point will emerge and replace the pure fixed point. However, if the pure fixed point is stable in the presence of weak disorder, a relation for the correlation length critical exponent ν of the pure system,

$$\nu \geq 2/d \,, \tag{1.24}$$

called the *Harris criterion* [12], must be satisfied.

Although weak random disorder is not guaranteed to be an irrelevant perturbation when Harris criterion is fulfilled, violating it, $\nu < 2/d$, means that the critical behavior of the phase transition in the disordered system, if exists, will be different from that of the pure system. The new critical exponent ν of the disorder system will still satisfy the Harris criterion [2,13,14]. We now show this relation, $\nu \geq 2/d$, for the critical exponent ν associated with transitions in disordered systems. Suppose the transition is controlled by a parameter x,

for example the concentration of impurities. By the very definition of the correlation length, the disordered system can be viewed as an ensemble of subsystems of size of the correlation length. From the *central limit theorem*, the typical fluctuation of x of a subsystem will be $\sim \left(\xi^d\right)^{-1/2} \sim \delta^{\nu d/2}$ where $\delta = |x - x_c|/x_c$. Self-consistency of the existence of a well-defined critical point requires that the typical statistical deviation $\delta^{\nu d/2}$ is smaller than δ, *i.e.*, the inequality $\nu \geq 2/d$ must hold. It should be clear that the above argument (actually the original argument developed by Harris) also implies that the Harris criterion, Eq. (1.24), must be satisfied if the weak disorder is an irrelevant perturbation on the pure fixed point.

The relation $\nu \geq 2/d$ for the SF-BG transition has important implication for the upper critical dimension, d_c, of this transition. Above d_c, hyperscaling breaks down because of *dangerously irrelevant operators* [24]. And the critical exponents take their mean-field values. Particularly, $\nu = 1/2$ for the correlation length and $\nu(d+z-2) = 1$ for the superfluid density. However, these mean-field critical exponents violate the relation $\nu \geq 2/d$, which implies that $d_c = \infty$ and that $z = d$ holds in all dimensions.

CHAPTER 2

THE PATH-INTEGRAL REPRESENTATION AND THE
WORM ALGORITHM

In this chapter, we will present the formalism of the path-integral representation widely used in directly simulating boson systems. Besides, we will introduce a mapping of the DBH model to a classical model, the J-current model, that can be used to efficiently study the critical physics. Our numerical studies in chapter 3 and chapter 4 will be based on materials presented here.

2.1   The path-integral representation

The central object in statistical physics is the partition function,

$$Z = \text{Tr} \, e^{-\beta H} \,, \tag{2.1}$$

where H is understood as the Hamiltonian minus the chemical potential term, μN, when calculating the grand canonical partition function. If we split the Hamiltonian into the hopping part and the potential energy part, $H = K + U$, the imaginary time evolution operator can be written in a compact way,

$$e^{-\beta H} = e^{-\beta U} \, T_\tau \, e^{-\int_0^\beta d\tau K(\tau)} \,, \tag{2.2}$$

where $K(\tau) = e^{\tau U} K e^{-\tau U}$ and T_τ is the time ordering operator.

The explicit form of the Dyson series for the time ordering part is (refer to [29] for example)

$$T_\tau \, e^{-\int_0^\beta d\tau K(\tau)} = \sum_{n=0}^{\infty} (-1)^n \int_{\tau_{n-1}}^\beta d\tau_n \cdots \int_{\tau_1}^\beta d\tau_2 \int_0^\beta d\tau_1 \, K(\tau_n) K(\tau_{n-1}) \cdots K(\tau_1) \,. \qquad (2.3)$$

In Fock basis where U is diagonal, the typical matrix element in calculating the partition function becomes

$$\left\langle \alpha_0 \left| e^{-\beta U} K(\tau_n) K(\tau_{n-1}) \cdots K(\tau_1) \right| \alpha_0 \right\rangle = \left\langle \alpha_0 \left| e^{-(\beta-\tau_n)U} K e^{-(\tau_n-\tau_{n-1})U} K \cdots e^{-(\tau_2-\tau_1)U} K e^{-\tau_1 U} \right| \alpha_0 \right\rangle$$

$$= \sum_{\alpha_1} \sum_{\alpha_2} \cdots \sum_{\alpha_{n-1}} e^{-(\beta-\tau_n)U_{\alpha_0}} K_{\alpha_0,\alpha_{n-1}} e^{-(\tau_n-\tau_{n-1})U_{\alpha_{n-1}}} K_{\alpha_{n-1},\alpha_{n-2}} \cdots e^{-(\tau_2-\tau_1)U_{\alpha_1}} K_{\alpha_1,\alpha_0} e^{-\tau_1 U_{\alpha_0}}$$

$$= \sum_{\alpha_1} \sum_{\alpha_2} \cdots \sum_{\alpha_{n-1}} e^{-\int_0^\beta U(\tau)d\tau} K_{\alpha_0,\alpha_{n-1}} K_{\alpha_{n-1},\alpha_{n-2}} \cdots K_{\alpha_1,\alpha_0} \,.$$

If we interpret $|\alpha_i\rangle$ as the state of the system from τ_i to τ_{i+1}, the imaginary time evolution of $|\alpha(\tau)\rangle$ from 0 to β subject to the boundary condition $|\alpha(\tau=0)\rangle = |\alpha(\tau=\beta)\rangle$ forms trajectories as shown in Fig. 2.1a. In this language, the partition function becomes the sum of the statistical weights of all trajectories. Take the DBH model for example. With $K = -t \sum_{\langle ij \rangle} (b_i^\dagger b_j + b_j^\dagger b_i)$, the partition function in Fock basis becomes

$$Z = \sum_{n=0}^{\infty} \int_{\tau_{n-1}}^\beta d\tau_n \cdots \int_{\tau_1}^\beta d\tau_2 \int_0^\beta d\tau_1 \sum_\nu W_{n,\nu} \,. \qquad (2.4)$$

And the explicit expression of $W_{n,\nu}$ is

$$W_{n,\nu} = \prod_{m=1}^n t\sqrt{n_j(\tau_m)[n_i(\tau_m)+1]} \exp\left\{ -\int_{\tau_{m-1}}^{\tau_m} d\tau \left(\frac{U}{2} \sum_i n_i(\tau)[n_i(\tau)-1] - \sum_i \mu_i n_i(\tau) \right) \right\} ,$$

where $n_i(\tau_m)$ is to be understood as the occupation number at time infinitesimal before τ_m. For positive t or bipartite lattices where only even values of n are allowed, the statistical

20

weights are always positive. Therefore, the path integral representation is well suited for Monte Carlo simulations. Moreover, a trajectory can be decomposed into a series of single particle propagating loops, called worldlines, that wind along imaginary time and spatial directions because of the particle number conservation law and periodic boundary condition. Configuration space consists of closed loops with positive weights can be then efficiently sampled by Worm algorithm [32–34]. Another advantage of the path integral representation

(a) The configuration space of the partition function consists of worldlines (the line thickness represents the site occupation number

(b) Worm algorithm sampling in the extended space of closed loops and one open line with two free ends.
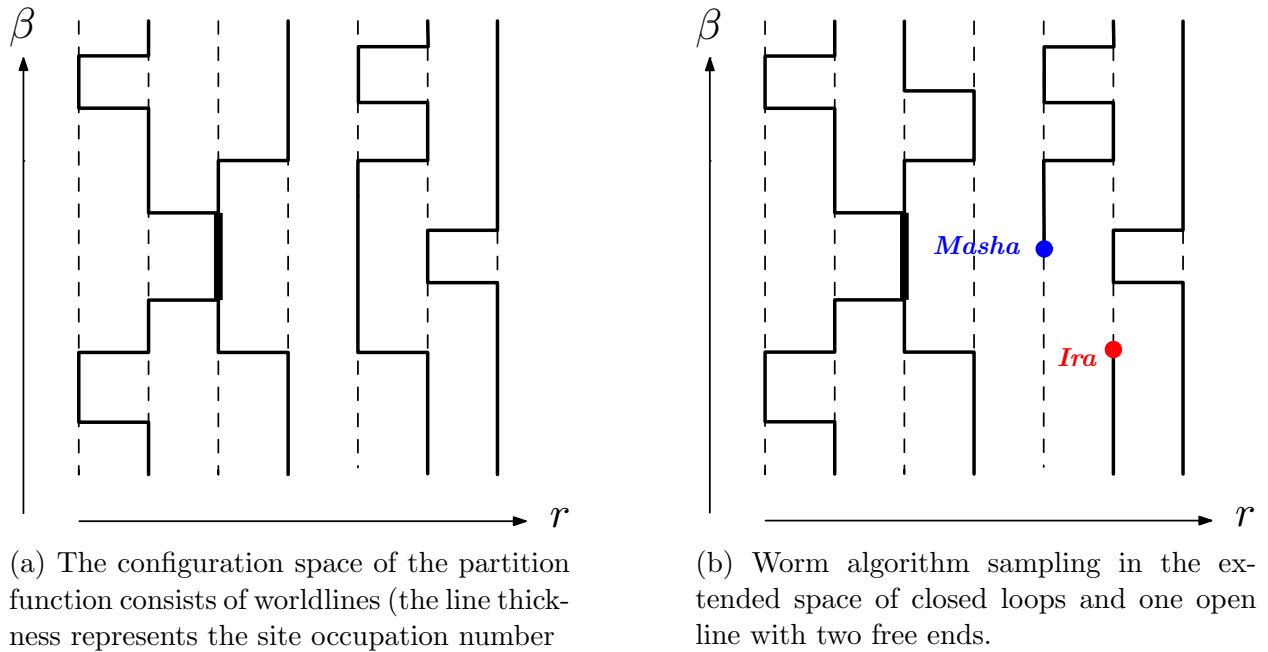
Figure 2.1: Path integral representation of the partition function of boson systems and the Worm algorithm.

is that the twisted boundary condition can be easily implemented. Similar to a elastic medium that the increase of the free energy under stretch or compression determines its elastic modulus, the free energy increase of a boson system under twisted boundary condition determines its superfluid stiffness, a measure of the "rigidity" of the phase field. The twisted boundary condition (a gauge flux of θ),

$$\oint \nabla\theta \cdot d\boldsymbol{\ell} = \theta + 2\pi M \,, \tag{2.5}$$

where M is an integer and the integral is to be understood in discrete sense, can be introduced by adding a phase factor of to the hopping amplitude,

$$t\, b_j^\dagger \, b_i \quad \rightarrow \quad t e^{i\theta_{ij}} \, b_j^\dagger \, b_i \,.$$

where $\theta_{ij} = \theta_j - \theta_i$. Since only closed loops (worldlines) contribute to the partition function, the phase factor associated with a trajectory will be $e^{iW\theta}$ where W is the winding number along the direction of the applied phase twist. Therefore, the partition function with the applied phase twist acquires the form,

$$Z(\theta) = \sum_W Z_W e^{iW\theta} \,, \tag{2.6}$$

where Z_W is the part of the partition function based on configurations with winding number W of the original system ($\theta = 0$). For a cubic system, the superfluid stiffness is given by

$$\Lambda_s = -k_B T \frac{L^2}{V} \left.\frac{\partial^2 \ln Z(\theta)}{\partial \theta^2}\right|_{\theta=0} = \frac{k_B T}{L^{d-2}} \langle W^2 \rangle = \frac{k_B T}{d L^{d-2}} \langle \mathbf{W}^2 \rangle \,, \tag{2.7}$$

where $\mathbf{W}^2 = \sum_{i=1}^d W_i^2$ is the sum of winding number squared along different spatial directions [31]. The number of worldlines has the meaning of total particle number in the system. The advantage of working in the grand canonical ensemble is that the compressibility defined as $\kappa = \partial n/\partial \mu$ can be computed from the particle number fluctuations of the system,

$$\kappa = \frac{\beta}{V} \left[\langle N^2 \rangle - \langle N \rangle^2 \right] \,. \tag{2.8}$$

2.2 J-current model

Although a quantum system can be directly simulated in path integral representation, it is still desirable to map the quantum system to a classical one as long as only the universal critical behavior is concerned. To find a mapping to a classical model, we start by considering the pure BH model. At large integer filling, the BH model can be quantitatively represented by the quantum rotor model,

$$H = -t \sum_{\langle ij \rangle} \cos(\theta_i - \theta_j) + \frac{U}{2} \sum_i L_i^2 , \tag{2.9}$$

where θ and L are canonical conjugated variables, $[\theta_i, L_j] = i\delta_{ij}$, and the eigenvalues of L_i are integers from $-\infty$ to $+\infty$. In Feynman's path integral representation [30], the partition function can be written as

$$Z = \int \mathcal{D}\theta \sum_L \exp[-S(\theta, L)] \tag{2.10}$$

with the action S given by

$$S = \sum_{i,m} -iL_i(\tau_m) \left[\theta_i(\tau_{m+1}) - \theta_i(\tau_m) \right] + \frac{U\Delta\tau}{2} \sum_{i,m} L_i^2(\tau_m) - t\Delta\tau \sum_{\langle ij \rangle,m} \cos\left[\theta_i(\tau_m) - \theta_j(\tau_m) \right]$$

where $\Delta\tau$ is the imaginary time spacing, i and m are the indices of the lattice site and imaginary time respectively. In the limit of vanishing $\Delta\tau$, the $\cos(\theta_i - \theta_j)$ term can be replaced with its Villain approximation [60] without changing the critical behavior,

$$e^{t\Delta\tau \cos(\theta_i - \theta_j)} \xrightarrow{\Delta\tau \to 0} \sqrt{\frac{2\pi}{K_\tau}} \sum_{n=-\infty}^{+\infty} \exp\left\{ -\frac{1}{2K_\tau}(\theta_i - \theta_j - 2\pi n)^2 \right\} , \quad K_\tau = 2\ln\frac{2}{t\Delta\tau} , \tag{2.11}$$

since the symmetry of the θ field is preserved. To integrate out the θ field, we rewrite the above Villain approximation using the Poisson summation formula,

$$\sum_{n=-\infty}^{+\infty} \sqrt{\frac{2\pi}{K}} e^{-\frac{1}{2K}(\theta_i - \theta_j - 2\pi n)^2} = \sum_{m=-\infty}^{+\infty} e^{-Km^2/2} e^{im(\theta_i - \theta_j)} . \tag{2.12}$$

Integration over θ is then straightforward and leaves us with a classical statistical model known as J-current model [61],

$$Z = \sum_{\{J_{n,\alpha}\}}' \exp\left[-\frac{1}{2}\sum_{n,\alpha} K_\alpha J_{n,\alpha}^2\right].$$ (2.13)

Here $n = (i,m)$ is the site index for the $(d+1)$-dimensional classical system, α enumerates space-time directions $\hat{x}, \hat{y}, \hat{z}, \cdots$ and $\hat{\tau}$, and $J_{n,\alpha}$ is the integer valued variable living on the bond connecting sites n and $n+\alpha$. The coupling parameters are related to the original parameters by $K_{\alpha=\hat{\tau}} = K_\tau = 2\ln\frac{2}{t\Delta\tau}$ and $K_{\alpha\neq\hat{\tau}} = U\Delta\tau$. The prime over the summation denotes the constraint on $J_{n,\alpha}$ imposed by integration over $\theta_i(\tau_m)$,

$$\sum_\alpha (J_{n,\alpha} + J_{n,-\alpha}) = 0$$ (2.14)

where the convention for $J_{n,-\alpha}$ is that $J_{n,-\alpha} = -J_{n-\alpha,\alpha}$. Graphically, this divergence-free condition for $J_{n,\alpha}$ translates to the condition of closed loops. As shown in Fig. 2.2, by associating positive and negative values with different directions, the configurations of this model become oriented loops, which naturally emerge in the study of the XY model by high-temperature expansions [67]. Moreover, with uniform spatial and temporal coupling constant $K_{n,\alpha} = K_\alpha$, this model is in the same universality class as the XY model. Physically, $J_{n,\tau}$ is particle number (deviation from the average to be more precise) of spatial site i from time τ_m to $\tau_m + \Delta\tau$, and $J_{n,\alpha}$ along the spatial direction ($\alpha \neq \hat{\tau}$) can be interpreted as spatial current. Then this divergence-free condition is a statement of the particle number conservation law. Because $J_{n,\hat{\tau}}$ is the particle occupation number, the diagonal disorder of the original DBH model can be implemented by adding a spatial-dependent disordered chemical potential term in Eq. (2.13). Still, the limit of $\Delta\tau \to 0$ poses a problem for numerical simulation. However, we can simply replace K_α by K since rescaling space and time is not expected to change

24
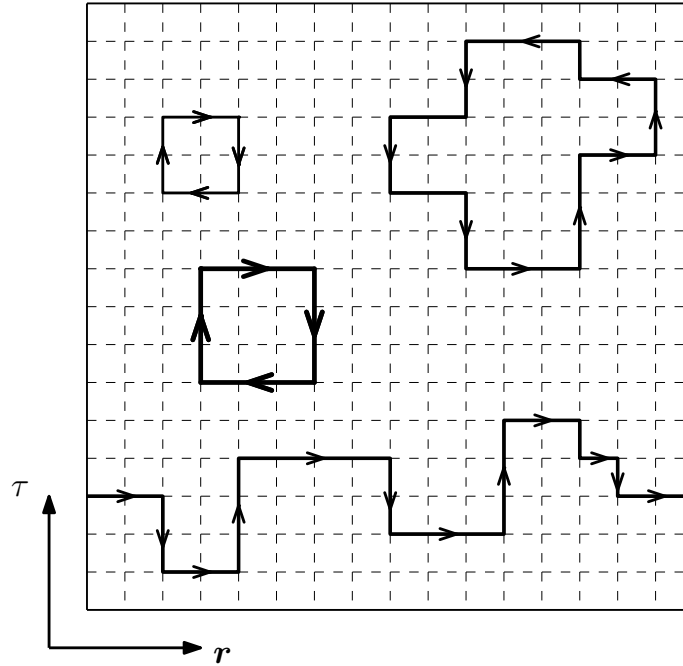
Figure 2.2: The configuration space of the J-current model consists of integer-valued closed loops. Here we represent a bond with positive $J_{n,\alpha}$ with an arrow pointing in the α direction and one with negative value with an arrow pointing in the $-\alpha$ direction. The width of a line is proportional to the value of $|J_{n,\alpha}|$.

the universal critical behavior [61]. One can then drive a phase transition by tunning the parameter K. The Hamiltonian of the classical system we will study in our simulation is therefore,

$$\beta H = K \sum_{n,\alpha}' J_{n,\alpha}^2 - \sum_n \mu_i J_{n,\tau} \,, \tag{2.15}$$

where $\mu_i = \mu + \delta\mu_i$ with $\delta\mu_i$ uniformly distributed within $[-\Delta, \Delta]$ and uncorrelated in space. By imposing a phase twist or equivalently a gauge field in the original system,

$$- t\cos(\theta_{i+1} - \theta_i) \quad \longrightarrow \quad -t\cos(\theta_{i+1} + \theta/L - \theta_i) \,, \tag{2.16}$$

and repeating the previous derivation, it is easy to show that the partition function and the "superfluid stiffness" of the J-current model have the same form as that of Eq. (2.6) and Eq. (2.7).

2.3 Worm algorithm for J-current model

Since the worm algorithm for simulating the quantum system in the path integral representation is well documented in the literature [32–34], we will focus on the worm algorithm for the J-current model. The essence of worm algorithm for models with configurations of closed loops is to enlarge the configuration space to include an open line (a worm) with two end points [72]. For our case, we will choose a directed line, and use the name Masha ($\mathcal{M}$) and Ira ($\mathcal{I}$) to encode the starting and end points respectively as shown in Fig. 2.3. The convention for the bond current carried by the open line is the same as those of closed loops. We will move the end points randomly and only collect statistics when $\mathcal{I} = \mathcal{M}$, i.e., when the configuration only consists of closed loops. Although being very simple, this worm update fulfills the ergodicity requirement. By choosing the same form of "Hamiltonian" for the statistical weight of states in the enlarged configuration space, the statistical weights of the physical states are also properly sampled.
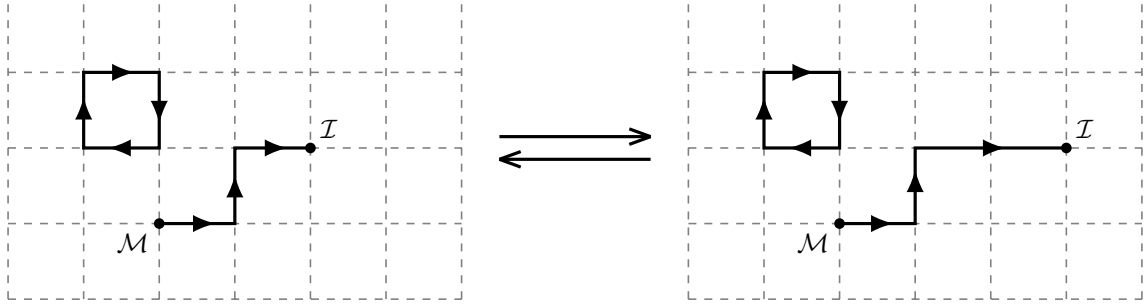
Figure 2.3: A typical Monte Carlo update in worm algorithm for the J-current model.

2.3.1   Complete algorithm

For numerical reasons, we will restrict the value of bond current in spatial directions to $[-J_r^{\text{Max}}, J_r^{\text{Max}}]$ and the value of bond current in temporal directions to $[J_\tau^{\text{Min}}, J_\tau^{\text{Max}}]$ without changing the universal physics near the critical point. Using υ to denote the direction of α or $-\alpha$, the complete algorithm is described as below.

1. PROPOSE

    - If no worm exists, select at random a new lattice site n to set $\mathcal{I} = \mathcal{M} = n$, a direction υ, and one end point, $\mathcal{I}$ or $\mathcal{M}$, to move in this direction;

    - If a worm exists, select at random $\mathcal{I}$ or $\mathcal{M}$, and a direction υ to move the chosen end point;

2. ACCEPT/REJECT

    - If the proposed end point is $\mathcal{I}$

        ○ If υ is in spatial directions and $J_{n,\upsilon} \neq J_r^{\text{Max}}$, determine the acceptance ratio R and accept the update with probability $\min\{R, 1\}$

        ○ If $\upsilon = \hat{\tau}$ and $J_{n,\upsilon} \neq J_\tau^{\text{Max}}$, or if $\upsilon = -\hat{\tau}$ and $J_{n,\upsilon} \neq -J_\tau^{\text{Min}}$, determine the acceptance ratio R and accept the update with probability $\min\{R, 1\}$

27

- If the proposed end point is $\mathcal{M}$

  ○ If υ is in spatial directions and $J_{n,\upsilon} \neq -J_r^{\mathrm{Max}}$, determine the acceptance ratio R and accept with probability $\min\{R, 1\}$

  ○ If $\upsilon = \hat{\tau}$ and $J_{n,\upsilon} \neq J_\tau^{\mathrm{Min}}$, or if $\upsilon = -\hat{\tau}$ and $J_{n,\upsilon} \neq -J_\tau^{\mathrm{Max}}$, determine the acceptance ratio R and accept the update with probability $\min\{R, 1\}$

3. COLLECT STATISTICS

  - Update $J_{n,\upsilon}$, $J_{n+\upsilon,-\upsilon}$ and $L_\alpha^{-1} \sum_n J_{n,\alpha}$, and collect statistics of winding numbers $W_\alpha = L_\alpha^{-1} \sum_n J_{n,\alpha}$ for $\alpha \neq \hat{\tau}$ and particle number $N = L_\tau^{-1} \sum_n J_{n,\hat{\tau}}$ if $\mathcal{I} = \mathcal{M}$.

2.3.2 Acceptance ratios

The Ira move in the direction of υ always changes $J_{n,\upsilon}$ to $J_{n,\upsilon} + 1$. If υ is in spatial directions, the acceptance ratio R is

$$R = \frac{W_{\nu'}}{W_\nu} = \exp\left\{-K(2J_{n,\upsilon} + 1)\right\} .$$

The acceptance ratios of Ira move in $-\hat{\tau}$ and $\hat{\tau}$ directions take different forms with

$$R = \frac{W_{\nu'}}{W_\nu} = \exp\left\{-K(2J_{n,\upsilon} + 1) \pm \mu_i\right\} ,$$

where the plus sign is for $\upsilon = -\hat{\tau}$ and the minus sign is for $\upsilon = \hat{\tau}$. The Masha move always changes $J_{n,\upsilon}$ to $J_{n,\upsilon} - 1$. The acceptance ratio in spatial directions is given by

$$R = \frac{W_{\nu'}}{W_\nu} = \exp\left\{K(2J_{n,\upsilon} - 1)\right\} .$$

In the case of temporal move, the acceptance ratios for $-\hat{\tau}$ and $\hat{\tau}$ directions are

$$R = \frac{W_{\nu'}}{W_\nu} = \exp\left\{K(2J_{n,\upsilon} - 1) \mp \mu_i\right\} ,$$

CHAPTER 3

CRITICAL EXPONENTS OF THE SF-BG TRANSITION IN THREE DIMENSIONS

In this chapter, we will closely follow Ref. [42] and present our results for the critical exponents of SF-BG transition in three dimensions, which resolved the critical-temperature exponent "crisis", $\phi \approx 1.1(1)$ and $\nu = 0.75(10)$, reported by Yu *et al.* [4, 5], and validated the quantum critical relations $\phi = \nu z$ and $z = d$.

3.1 The ϕ-exponent "crisis"

As have been discussed in the first chapter, based on scaling arguments and the fact that κ is finite at the critical point of the quantum SF-BG transition, it was predicted that the dynamic critical exponent, z, always equals the dimension of space; i.e., $z = d$ [7]. And the critical temperature exponent for the SF-NL transition satisfies the relation $\phi = \nu z$. Therefore, with the Harris criterion $\nu \geq 2/d$ [12, 14] for the correlation length exponent in disordered systems taken into consideration, it is expected that $\phi \geq 2$, within the standard picture of quantum critical phenomena.

Despite substantial research efforts in the last two decades, some aspects of the universal critical behavior described above remain controversial (see, e.g., Ref. [11]). For instance, Ref. [6] argues that finite κ at the SF-BG critical point might come from the regular analytic (rather than singular critical) part of the free energy, and, thus, $z < d$ should be considered as an undetermined critical exponent. Moreover, recent experiments on magnetic systems [4], as well as quantum Monte Carlo simulations of related disordered $S = 1$ antiferromagnets with

29

single-ion anisotropy [5], which use magnetic field (equivalent to the chemical potential in the bosonic system) as a control parameter to drive the system to quantum criticality, report compelling evidence that the values $\phi \approx 1.1(1)$ and $\nu \approx 0.75(10)$ are in strong violation of the key relation $\phi = z\nu$ and the bound $\phi \geq 2$. As a result, finite-temperature scaling relations used to describe SF-BG criticality for decades, are challenged.

3.2 Numerical study of the hard-core DBH model

Consider the hard-core DBH on the simple cubic lattice (equivalent to the spin-1/2 XY-ferromagnet in magnetic field) with the Hamiltonian

$$H = -t \sum_{\langle ij \rangle} \left(b_i^\dagger b_j + h.c. \right) - \sum_i (\mu + \delta\mu_i) n_i . \tag{3.1}$$

The symbols carry the same meanings as those in Eq. (1.7), and $\delta\mu_i$ is also uniformly distributed on the $[-\Delta, \Delta]$ interval and uncorrelated in space. The only difference is the hard-core constraint $n_i \leq 1$ as a consequence of infinite U in the original model. The SF-BG transition is induced by fixing disorder strength at $\Delta/t = 16$ and decreasing the chemical potential, similarly to the protocol employed in Refs. [4,5,11]. Our data for $T_c(\mu)$ are shown in Fig. 3.1. They feature an extended region in the parameter space where $T_c(\mu)$ is decreasing by closely following the reported $(\mu - \mu_c)^{1.1}$ law. However, with highly accurate data for T_c (our system sizes are at least an order of magnitude larger than in previous work) we observe that the last point is deviating from this power-law well outside of its error bar, see inset in Fig. 3.1, indicating that most of the points in Fig. 3.1 might not be in the critical regime yet. This observation is confirmed by revealing the $n(\mu)$ dependence in Fig. 3.2. Since density remains finite at the QCP, one requirement of being in the quantum critical region is to have $n(\mu) - n(\mu_c) \ll n(\mu_c)$. This condition is clearly violated for most of the points used to establish the $T_c \propto (\mu - \mu_c)^{1.1}$ law in previous studies at low fields.
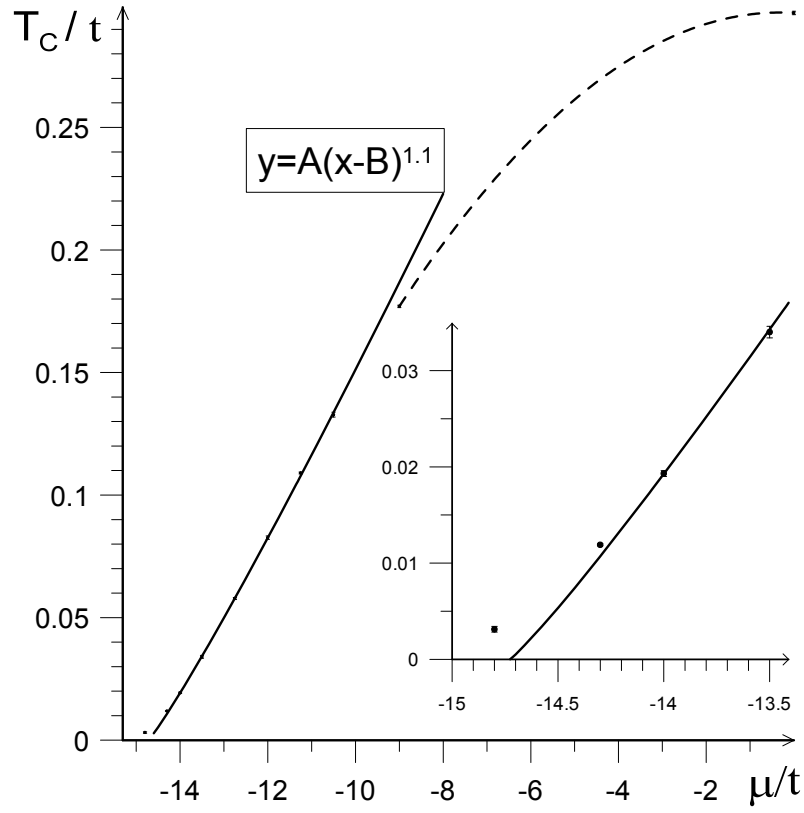
Figure 3.1: Critical temperature of the hard-core Bose-Hubbard model as a function of chemical potential for disorder strength $\Delta/t = 16$ fitted to the $T_c = A(\mu - \mu_c)^{1.1}$ power law. The dashed line is to guide an eye.
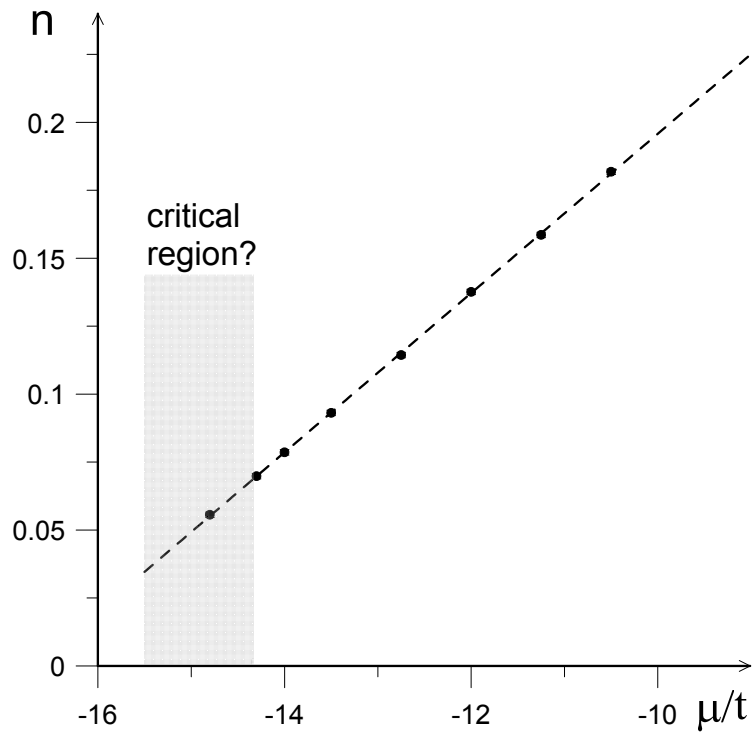
Figure 3.2: Density at the thermal critical point of model (3.1) as a function of chemical potential for $\Delta/t = 16$. The dashed line is a linear fit.

3.3 Critical exponents of the SF-BG transition in three dimensions

Since current problems with scaling relations are likely originating from strong $n(\mu)$ dependence when μ is used as a control parameter (leading to the critical region with extremely small T_c values), we radically change the strategy and study the SF-BG criticality as a function of disorder strength Δ at constant density. Universal properties of QCPs in d-dimensions can be equally well studied using $(d+1)$-dimensional classical mappings which are algorithmically superior from the numerical point of view. Therefore, we performed our simulation on the J-current model (2.15) with constraints $J_{n,\alpha=\tau} = 0, 1$ and $J_{n,\alpha\neq\tau} = -1, 0, 1$ to further speed up simulation. Since commensurability is not relevant for the SF-BG criticality [64, 65], we simulate our model (2.15) with $K = 2$ at half-integer filling factor, when $\mu = K$.

Accurate determination of the critical exponent ϕ ultimately rests on precise location of the QCP, or critical disorder strength Δ_c, where the power law originates. [Otherwise, one can be easily mislead by the transient behavior (similarly to one shown in Fig. 3.1). Likewise, all data points for the J-current model can be fit nearly perfectly with the power law based on $\phi \approx 3.3$ if Δ_c is kept as a free parameter.] To determine Δ_c along with the correlation length exponent ν, we employ FSS of scale-invariant mean-square winding number fluctuations,

$$\langle W^2 \rangle = \frac{1}{d} \sum_{\alpha=x,y,z} \langle W_\alpha^2 \rangle \; , \tag{3.2}$$

where $W_\alpha = 1/L_\alpha \sum_n J_{n,\alpha}$ is the winding number in α direction. If small detuning from the QCP is characterized by $\delta = (\Delta_c - \Delta)/\Delta_c$, then the correlation lengths in space and time directions, ξ and ξ_τ, diverge as $\xi_\tau \propto \xi^z \propto |\delta|^{-\nu z}$, and $\langle W^2 \rangle$ is a universal function of length scale ratios

$$\langle W^2 \rangle = f(L/\xi, L_\tau/\xi_\tau) = \tilde{f}(L^{1/\nu}\delta) \; . \tag{3.3}$$

In the last equality we assume that the ratio L_τ/L^z is fixed. By plotting $\langle W^2 \rangle$ for different system sizes, one determines the critical parameter from the crossing point of $\tilde{f}$ curves (if z was guessed correctly). As can be seen from Fig. 3.3, our FSS data are in perfect agreement with the scaling relation $z = d$ established in [7].

For FSS at the QCP we fix $L_\tau/L^3 = 2$ and consider only large system sizes from $N = 2 \times 12^6$ to $N = 2 \times 20^6$ sites (we hit the limit of what modern computer cluster can handle in reasonable time, given that every parameter point has to be averaged over $5000 - 20000$ disorder realizations). The crossing of $\tilde{f}$-curves shown in Fig. 3.3 pinpoints the critical disorder strength to be at $\Delta_c = 9.02(5)$.
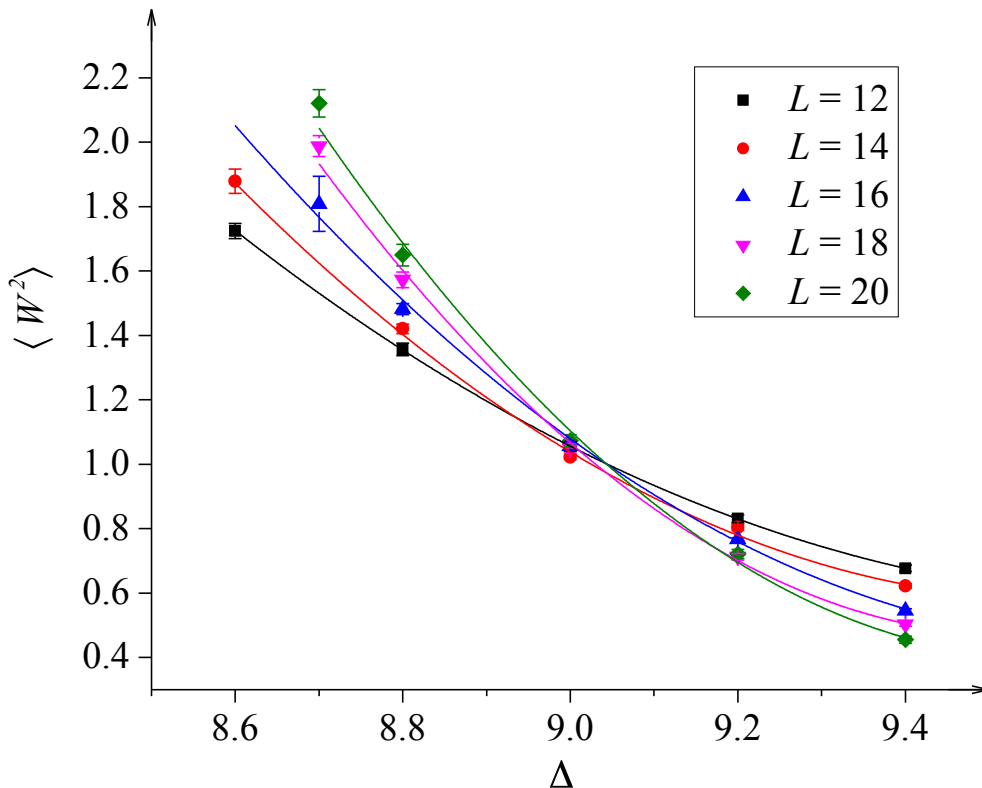
Figure 3.3: Finite-size scaling plots for $\langle W^2 \rangle = \tilde{f}(L^{1/\nu}\delta)$ for system sizes $L = 12$ (black), $L = 14$ (red), $L = 16$ (blue), $L = 18$ (magenta), and $L = 20$ (green) with fixed ratio $L_\tau = 2L^3$. Data points are fitted with second-order polynomials. We do not observe corrections to scaling within our error bars.

From Eq. (3.3), it follows that at the critical point

$$\partial \langle W^2 \rangle / \partial \Delta = const \times L^{1/\nu} \,, \tag{3.4}$$

enabling one to determine the correlation length exponent ν from the slopes of universal curves at the crossing point. The corresponding analysis is shown in Fig. 3.4 where $\nu = 0.88(5)$ is deduced from the log-log plot of $\tilde{f}$ derivatives. This result is in full agreement with previous findings [5, 71].
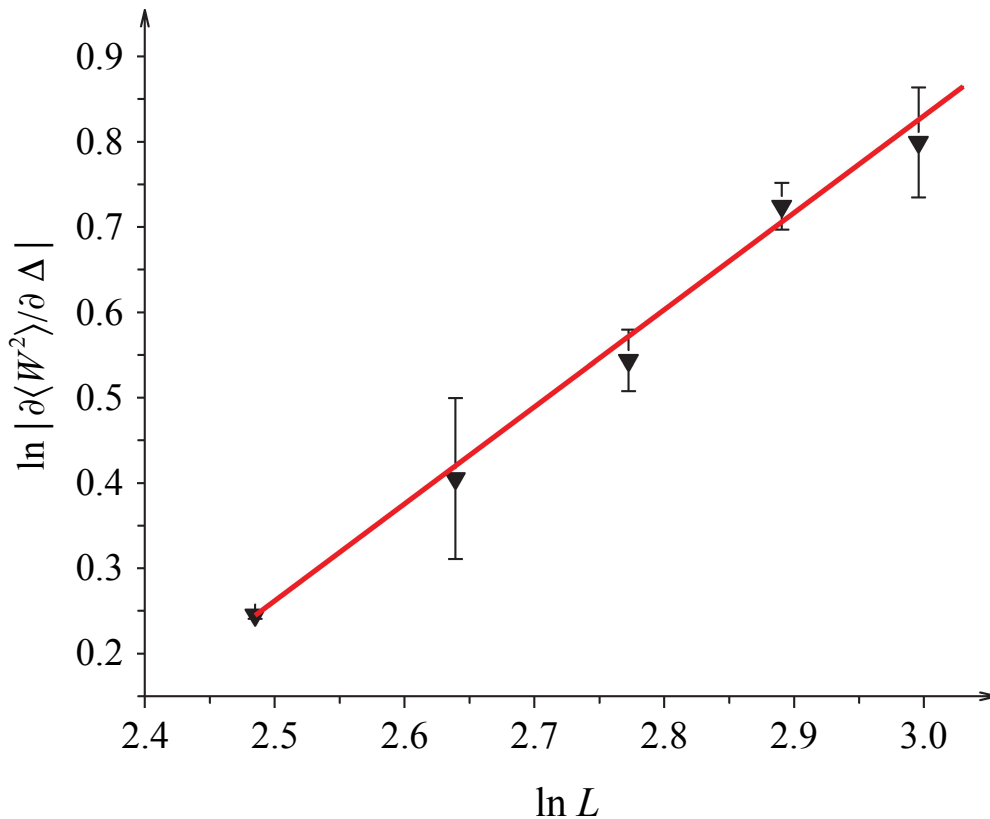
Figure 3.4: Deducing $1/\nu$ from the linear fit of $\ln |\partial \langle W^2 \rangle / \partial \Delta|$ as a function of $\ln L$ using 4 points near the critical point, $\Delta = 8.8, 9.0, 9.2, 9.4$. Error bars are based on the uncertainty of the fitting procedure, given the data points and their statistical error bars in Fig. 3.3.

We now proceed to the evaluation of the critical-temperature exponent ϕ from accurate measurements of $T_c(\Delta)$ (using similar FSS analysis) and the power-law $T_c = A\delta^\phi$ fit to the

lowest transition temperatures, see Fig. 3.5. In striking contrast to Fig. 3.1 and previously reported results [4, 5], all data points nicely follow the power-law curve $T_c \propto (8.83 - \Delta)^{3.27}$ as T_c decreases nearly two orders in magnitude! If Δ_c were left undetermined we would have to conclude that $\phi \approx 3.3$. However, if the power-law fit is performed with the known value of QCP (i.e., with $\Delta_c = 9.02$), the prediction is different: The ϕ exponent decreases from 2.9 to 2.7 as we reduce the number of the lowest-temperature points to be included in the fit from $T_c < 0.1$ to $T_c < 0.01$. We thus claim our final result as $\phi = 2.7(2)$, which is in good agreement with the prediction based on the quantum critical relation $\phi = z\nu$ with $z = 3$ and $\nu = 0.88(5)$. [The order parameter exponent deduced from the constant-density approach, $\beta = 1.50(2)$, also differs significantly from the value $\beta \approx 0.6(1)$ characteristic of the transient $\mu/t \geq -14$ interval.]

To verify the universality of our findings and to shed light on what to expect if a similar study is attempted experimentally using magnetic or cold-atom systems, we performed quantum Monte Carlo simulation of model (3.1) at half-integer filling factor (i.e., at $\mu = 0$, or zero external magnetic field in the case of spin-1/2 XY-ferromagnet). Our data for normal-to-superfluid transition temperature as a function of disorder strength are shown in Fig. 3.6 ($T_c(\Delta)$ was determined from FSS analysis of $\langle W^2 \rangle$ plots with $8 \leq L \leq 64$). Given that simulations of quantum models are more challenging numerically, we did not attempt to determine Δ_c and averaged results over smaller number of disorder realizations, from 5000 at high temperature to 500 at low temperature. The lowest transition temperatures can be perfectly fitted to the $T_c \propto (\Delta_c - \Delta)^{2.7}$ law with $\Delta_c/t = 24.67$. This critical behavior starts at temperatures as high as $T_c/t < 0.5$ and we were able to verify it down to $T_c/t \approx 0.03$, see Fig. 3.6 inset. There is no doubt that the $\phi > 2$ condition is satisfied at the SF-BG transition.
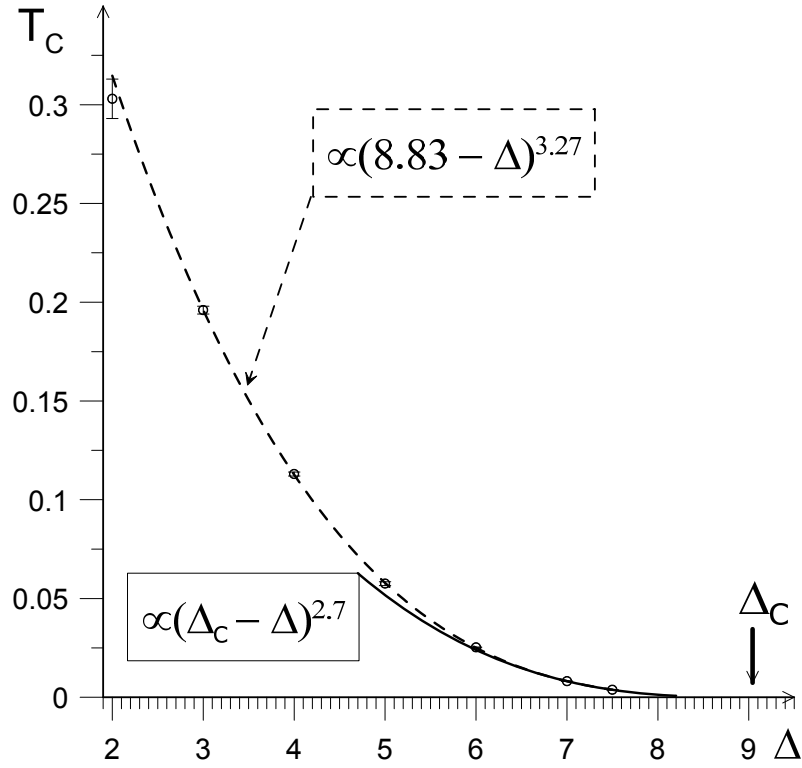
Figure 3.5: Critical temperature of the J-current model as a function of disorder strength. Solid line is the power-law fit to the lowest transition temperatures assuming known location of the quantum critical point. Dashed line is a power-law originating from $\Delta = 8.83$.
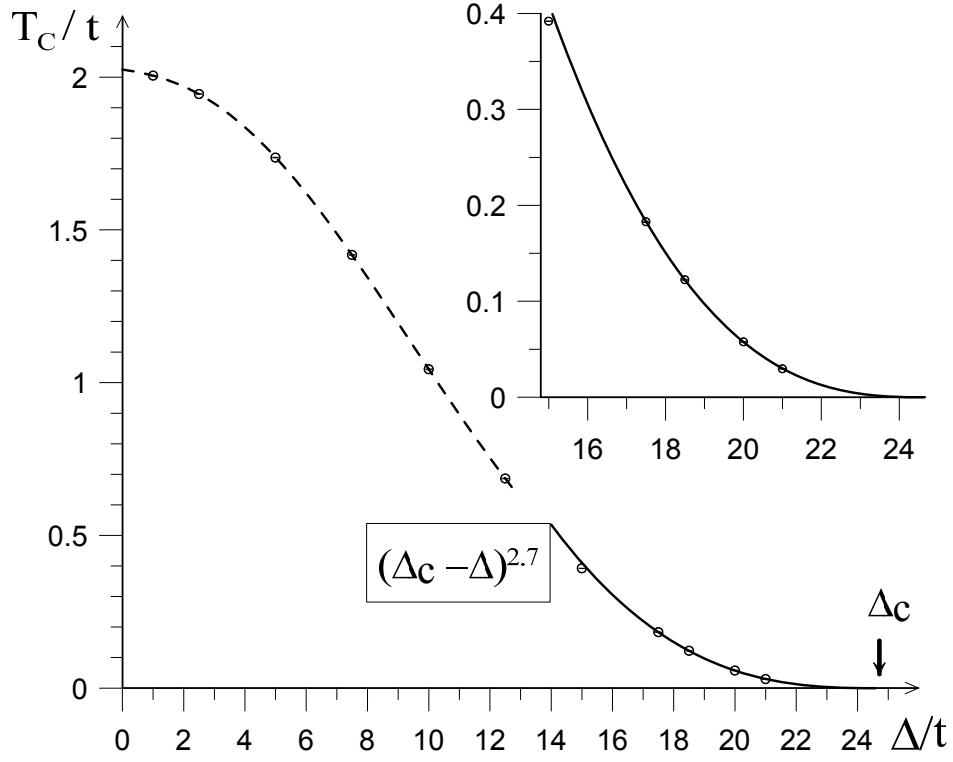
Figure 3.6: Critical temperature dependence on disorder strength in the hard-core DBH at half-integer filling factor. The solid line is a fit of the last five points to the $A(\Delta_c - \Delta)^\phi$ law with exponent $\phi = 2.7$ fixed at the value determined from simulations of the J-current model. From this fit we predict that the quantum critical point is located at $\Delta_c \approx 24.67$. Error bars are shown but are smaller than the symbol size. Inset: Zoom in to the tail of the main plot.

3.4 Concluding remarks

In summary, we addressed the current ϕ-exponent "crisis" for the superfluid-to-Bose Glass universality class in three dimensions. Previous work questioned conventional scaling relations $z = d$ and $\phi = z\nu$ with $\nu > d/2$ for the SF-BG quantum critical point. Using extensive Monte Carlo simulations of the hard-core DBH and its classical J-current counterpart we were able to identify problems with previous analysis (strong dependence of density/magnetization on chemical potential/external magnetic field on approach to quantum criticality). We argued that $z = d$ as an exact relation, and used it to determine the critical-temperature exponent ϕ from simulations of the J-current model. Our final result $\phi = 2.7(2)$ is in good agreement with the quantum critical prediction $\phi = z\nu = d\nu$ based on $\nu = 0.88(5)$, putting the controversy to an end. We verified universality of our findings and determined under what conditions the ϕ exponent can be studied experimentally.

CHAPTER 4

SUPERFLUID–BOSE-GLASS QUANTUM PHASE
TRANSITION IN ONE DIMENSION

In this chapter, we will first introduce several important concepts, such as Luttinger liquid theory and Kane-Fisher renormalization, essential for our later discussion. We will then present an asymptotically exact theory renormalization-group theory of the superfluid-insulator transition in 1D disordered systems, analyze the interplay between the Giamarchi-Schulz (instanton–anti-instanton) and weak-link (scratched-XY) criticalities, and present our numerical results on one-dimensional DBH model at unit filling. A large portion of the material in this chapter is adapted from [58].

4.1   Luttinger liquid theory

In 1960, Girardeau established that in one dimension there is no qualitative difference between fermions and bosons: spinless fermions can be exactly mapped to hard-core bosons [35]. Later, Haldane established that the low energy physics of 1D quantum liquids, bosonic and fermionic, can be generically described by a quadratic fixed point Hamiltonian—the Luttinger liquid (LL) Hamiltonian [36,37]. For example, the number difference of right and left moving fermions can be identified as the phase winding number of a superfluid, and the backscattering events of a fermion system correspond to the quantum phase slippages of a bosonic superfluid. The underlying reason behind this generic LL description lies in a unified description of the long-wavelength density fluctuation of 1D quantum liquids. Formally, we

can introduce a *phonon displacement field*, $\theta_l(x)$, which takes the value of $2\pi n$ at the position, x_n, of the n-th particle. The density operator can then be expressed in terms of the θ_l field,

$$\rho(x) = \sum_{n=-\infty}^{\infty} \delta(x - x_n) = \sum_{n=-\infty}^{\infty} |\nabla\theta_l(x)| \, \delta(\theta_l(x) - 2\pi n) = \frac{\nabla\theta_l(x)}{2\pi} \sum_{p=-\infty}^{\infty} e^{ip\theta_l(x)}, \qquad (4.1)$$

where θ_l is a monotonically increasing function by construction (∇ is to be understood as d/dx in one dimension) [38]. It is useful to define a new field $\theta(x) = (\theta_l(x) - 2\pi\rho_0 x)/2$ with ρ_0 the average density that represents the deviation from the perfect state in which all the particles are evenly spaced. In this way, the density operator becomes

$$\rho(x) = \left[\rho_0 + \frac{1}{\pi}\nabla\theta(x)\right] \sum_{p=-\infty}^{\infty} e^{i2p(k_F x + \theta(x))}. \qquad (4.2)$$

where $k_F = \pi\rho_0$. Clearly, the $p = 0$ term corresponds to the long-wavelength smeared density, $\rho_{q\sim 0}(x) \approx \rho_0 + \nabla\theta(x)/\pi$ with $\nabla\theta(x)/\pi$ as the smeared density fluctuation. As usual, the bosonic field operator can be written as $\psi_B^\dagger(x) = [\rho(x)]^{1/2} e^{-i\phi(x)}$ using density and phase fields. By making use of Eq. (4.2), the field operator $\psi_B^\dagger(x)$ can be parameterized as [39]

$$\psi_B^\dagger(x) = \left[\rho_0 + \frac{1}{\pi}\nabla\theta(x)\right]^{1/2} \sum_{p=-\infty}^{\infty} e^{i2p(k_F x + \theta(x))} e^{-i\phi(x)}. \qquad (4.3)$$

The commutation relation between $\phi(x)$ and $\theta(x')$,

$$[\phi(x), \theta(x')] = \frac{i\pi}{2}\text{sgn}(x - x'), \qquad (4.4)$$

follows from that of the bosonic field operators. With the field representation of the bosonic field operator, the fermionic one can be obtained by a Jordan-Wigner transformation,

$$\psi_F^\dagger(x) = \left[\rho_0 + \frac{1}{\pi}\nabla\theta(x)\right]^{1/2} \sum_{p=-\infty}^{\infty} e^{i(2p+1)(k_F x + \theta(x))} e^{-i\phi(x)}. \qquad (4.5)$$

Therefore, quite generally, for both bosonic and fermionic systems, the low-energy physics of a one-dimensional quantum liquid (LL) can be described by the θ and ϕ fields. Assuming inversion symmetry, we arrive at the quadratic LL Hamiltonian,

$$H = \frac{\hbar}{2\pi} \int dx \left[uK(\nabla\phi)^2 + \frac{u}{K}(\nabla\theta)^2 \right] ,$$

(4.6)

where K is the LL parameter and u is the renormalized velocity. A comparison of the LL Hamiltonian with the low-energy effective Hamiltonian of a superfluid,

$$H = \int dx \left[\frac{\Lambda_s}{2} \left(\nabla\phi(x) \right)^2 + \frac{(\delta n)^2}{2\kappa} \right] ,$$

(4.7)

enables us to relate u and K to Λ_s and κ,

$$u = \sqrt{\Lambda_s/\kappa\hbar^2} = \sqrt{n_s/m\kappa} , \quad K = \pi\sqrt{\Lambda_s\kappa} = \pi\hbar\kappa u ,$$

(4.8)

where n_s is the superfluid number density and m is the mass of one atom of the superfluid.

4.2   Giamarchi-Schulz renormalization

In this section we will briefly review the SF-I transition of a one-dimensional disordered boson system in the weak disorder limit. The presence of weak on-site disorder (impurities) can be described by adding the following perturbation,

$$H_1 = \int dx\rho(x)V(x) ,$$

(4.9)

to the LL Hamiltonian where $V(x)$ is the disorder potential. In the limit of weak and dense impurities, the distribution of $V(x)$ can be treated as a Gaussian distribution from the *central*

limit theorem,

$$P(\{V(x)\}) \propto e^{-\frac{1}{2D} \int dx\, V^2(x)}\,, \quad \overline{V(x)V(x')} = D\delta(x - x')\,, \tag{4.10}$$

where the overline stands for the average with respect to the disorder distribution, and D is a constant characterizing the strength of the disorder. If we, in the language of fermions, keep the most important forward and backscattering terms (will be confirmed later), the perturbation becomes

$$H_1 = \int dx \left[\frac{\nabla\theta(x)}{\pi} \eta(x) + \rho_0 \left(\xi(x)e^{2i\theta(x)} + \xi^*(x)e^{-2i\theta(x)} \right) \right]. \tag{4.11}$$

Here the fields η and $\xi(\xi^*)$ responsible for forward and backscattering processes respectively are subject to Gaussian distributions with,

$$\overline{\eta(x)\eta(x')} = D_f\, \delta(x - x'), \qquad \overline{\xi(x)\xi^*(x')} = D_b\, \delta(x - x')\,. \tag{4.12}$$

At the Hamiltonian level, the forward scattering term can be absorbed into the LL Hamiltonian by a shift of $\theta(x)$ and a redefinition of $\xi(x)$,

$$\tilde{\theta}(x) = \theta(x) + \frac{K}{u} \int_0^x \eta(x')dx'\,, \quad \tilde{\xi}(x) = \xi(x)e^{i\frac{2K}{u}\int_0^x \eta(x')dx'}\,. \tag{4.13}$$

A constant phase shift of $\xi(x)$ does not change the distribution of the field, and we will write $\tilde{\xi}(x)$ as $\xi(x)$ for notational convenience from now on. As usual, in studying the physics of disordered systems, we will use the *replica method* to study the problem of n replicas. The action of n replicas in θ representation is

$$S_n[\{\theta\}] = \sum_{i=1}^n S_0[\theta_i] - \rho_0^2 D_b \sum_{i,j=1}^n \int dx \int d\tau \int d\tau' \cos(2\theta_i(x,\tau) - 2\theta_j(x,\tau'))\,, \tag{4.14}$$

where $S_0[\theta]$ is the action of the pure LL after integrating out the phase fluctuations,

$$S_0[\theta] = \frac{1}{2\pi K} \int dx \int d\tau \left[u(\nabla\theta(x,\tau))^2 + \frac{1}{u}(\partial_\tau\theta(x,\tau))^2 \right] . \qquad (4.15)$$

To derive the RG equations, we split the field into fast and slow modes, $\theta(x,\tau) = \theta_f + \theta_s$,

$$\theta_f(x,\tau) = \frac{1}{\beta L} \sum_{\Lambda' < |\boldsymbol{q}| < \Lambda} e^{i(kx-\omega_n t)}\theta(k,\omega_n), \qquad (4.16)$$

$$\theta_s(x,\tau) = \frac{1}{\beta L} \sum_{|\boldsymbol{q}| < \Lambda'} e^{i(kx-\omega_n t)}\theta(k,\omega_n), \qquad (4.17)$$

where $\boldsymbol{q} = (k,\omega_n)$ and $\Lambda(\Lambda')$ is ultraviolet momentum-frequency cutoff. After expanding the exponential of S_1 to first order,

$$Z = \int \prod_{i=1}^{n} \mathcal{D}\theta_i \, e^{-S_0-S_1} \approx \int \prod_{i=1}^{n} \mathcal{D}\theta_i \, e^{-S_0}(1-S_1), \qquad (4.18)$$

and averaging out the fast modes, the diagonal term (replica indices $i = j$) takes the following form,

$$\rho_0^2 D_b \int dx d\tau d\tau' \, \cos(2\theta_s(x,\tau) - 2\theta_s(x,\tau')) e^{-\frac{4}{\beta L} \sum_{\Lambda' < |\boldsymbol{q}| < \Lambda} [1-\cos(\tau-\tau')\omega_n]\frac{\pi K u}{\omega_n^2 + u^2 k^2}} . \qquad (4.19)$$

Since the term in the exponential is fast decaying, the main contribution comes from small $|\tau - \tau'|$. The expansion of $\cos(2\theta_s(x,\tau) - 2\theta_s(x,\tau'))$ in $|\tau - \tau'|$ generates a quadratic term $(\partial\theta/\partial\tau)^2$ which renormalizes $\frac{1}{2\pi K u}$,

$$\frac{1}{2\pi K(\infty)u(\infty)} = \frac{1}{2\pi K(\alpha)u(\alpha)} + \rho_0^2 D \int_\alpha^\infty 4\tau^2 \left(\frac{\tau}{\alpha}\right)^{-2K} d\tau, \qquad (4.20)$$

44

where α is the ultraviolet cutoff in imaginary time. Meanwhile, the value of $\frac{u}{2\pi K}$ is not renormalized in this order. Therefore, the full set of leading order RG equations are,

$$\frac{d\tilde{D}}{d\ell} = (3 - 2K)\tilde{D}\,, \tag{4.21}$$

$$\frac{dK}{d\ell} = -\frac{K^2}{2}\tilde{D}\,, \tag{4.22}$$

$$\frac{du}{d\ell} = -\frac{uK}{2}\tilde{D}\,, \tag{4.23}$$

where $\tilde{D} \propto \rho_0^2 u D_b$ represents the strength of disorder. According to Eq. (4.8), the superfluid stiffness is always renormalized down, while the compressibility remains the same under RG flow. As discussed in chapter 2, the superfluid stiffness and the compressibility are related to the free energy response of phase twists in spatial and temporal directions respectively. If we attribute the renormalization effects to vortexes in a two-dimensional classical system, this implies that only vertical vortex–anti-vortex pairs are contributing to the renormalization, a point will be confirmed later.

On one hand, it is clear that $\tilde{D}$ begins to increase indefinitely whenever the condition $K(\ell) < 3/2$ is fulfilled, signaling that the thermodynamic state of the system is an insulating state. On the other hand, if the condition $K(\ell) < 3/2$ is never met, the system will flow to a pure LL fixed point with $K(\infty) > 3/2$ and $\tilde{D}(\infty) = 0$. Therefore, there is a SF-I transition with universal critical LL parameter $K_c = 3/2$. The fact that K_c is universal indicates that the critical condition is valid beyond the weak disorder limit. However, whether this condition determines the whole SF-I transition line or it is only valid up to a multicritical point beyond which a new universality class takes over is out of the reach of this perturbative RG approach.

4.3 Kane-Fisher renormalization

Having examined the limit of weak and dense impurities, we now switch to discuss the physics of a single impurity in an otherwise pure LL [43,44]. Let us first consider the case of a strong barrier (tunnel junction) placed at $x = 0$. In zeroth-order approximation, the system is composed of two disconnected Luttinger liquids, which is described by the Hamiltonian,

$$H_0 = \frac{\hbar}{2\pi} \int_{-\infty}^{0} \left[uK(\nabla\phi_1)^2 + \frac{u}{K}(\nabla\theta_1)^2 \right] + \frac{\hbar}{2\pi} \int_{0}^{\infty} \left[uK(\nabla\phi_2)^2 + \frac{u}{K}(\nabla\theta_2)^2 \right] . \quad (4.24)$$

The effect of a strong but finite barrier is to introduce particle hopping across the barrier, *i.e.*, a perturbation

$$H_1 = -t \left(\psi_1^\dagger(x = 0)\psi_2(x = 0) + \text{H.c.} \right) . \quad (4.25)$$

Here t is the hopping amplitude, and $t = 0$ corresponds to the limit of infinite strong barrier. After integrating out the θ field, the partition function in the ϕ field representation is

$$Z = \int \mathcal{D}\phi_1 \mathcal{D}\phi_2 \, e^{-S[\phi_1,\phi_2]} = \int \mathcal{D}\phi_1 \mathcal{D}\phi_2 \, e^{-S[\phi_1(x,\tau),\phi_2(x,\tau)]} \quad (4.26)$$

where the action S is given by

$$S[\phi_1, \phi_2] = \sum_{i=1,2} \frac{K}{2\pi} \int dx_i \, d\tau \left[u(\nabla\phi_i)^2 + \frac{1}{u}(\partial_\tau\phi_i)^2 \right] - t \int d\tau \cos(\phi_1(0,\tau) - \phi_2(0,\tau)). \quad (4.27)$$

To obtain the RG equation for t, we need to integrate out the ϕ_i field at all positions except for the point $x = 0$. This can be done by introducing two auxiliary fields $\varphi_i(\tau)$ for $i = 1, 2$ satisfying $\varphi_i(\tau) = \phi_i(x = 0, \tau)$ and then integrating out the original $\phi_i(x, \tau)$ field so that the

partition function is written in terms of $\varphi_i(\tau)$ field [45]. Following this procedure, we arrive at the partition function,

$$Z \propto \int \mathcal{D}\varphi \exp\left[-\frac{K}{\pi}\sum_\omega |\omega|\varphi^*(\omega)\varphi(\omega) + t\int d\tau \cos 2\varphi(\tau)\right], \tag{4.28}$$

where $\varphi = (\varphi_1 - \varphi_2)/2$ is half of the phase difference across the barrier. The scaling dimension of the operator $\cos 2\varphi$ can be determined by splitting the field into fast and slow modes, $\varphi = \varphi_f + \varphi_s$, and integrating out the fast modes,

$$\langle \cos 2(\varphi_f + \varphi_s)\rangle_f = b^{-\frac{1}{K}} \cos 2\varphi_s, \tag{4.29}$$

where b is the RG rescaling factor $b = e^{d\ell}$. Therefore, the scaling dimension of the operator $\cos 2\varphi$ is $1/K$, and the leading order RG equation for t is

$$\frac{dt}{d\ell} = (1 - \frac{1}{K})t. \tag{4.30}$$

The LL parameter K is not renormalized at all orders in perturbation theory since the hopping perturbation is local while K is the global coupling parameter.

In the opposite limit of weak impurity, the system can be viewed as a pure LL with the perturbation,

$$H_1 = \int dx\, \rho(x)V(x) = \int dx \left[\rho_0 + \frac{1}{\pi}\nabla\theta(x)\right] \sum_{n=-\infty}^{\infty} e^{i2n(k_F x + \theta(x))}V(x), \tag{4.31}$$

where $V(x)$ is centered around $x = 0$. The contribution of H_1 to the action is

$$S_1 \approx \sum_{n=-\infty}^{\infty} \rho_0 V_{-n} \int d\tau\, e^{i2n\theta(x=0,\tau)}, \tag{4.32}$$

47

where V_n is the n-th Fourier component of $V(x)$. This problem is dual to that of the strong barrier, and the renormalization equation for V_n is

$$\frac{dV_n}{d\ell} = (1 - n^2 K)V_n \,. \tag{4.33}$$

Since free fermions correspond to $K = 1$, combining Eq. (4.30) and Eq. (4.33) enables us to connect the RG flow in regions inaccessible by the perturbative RG method. The RG flow is shown in Fig. (4.1). Therefore, regardless of the strength of the impurity , the perturbation
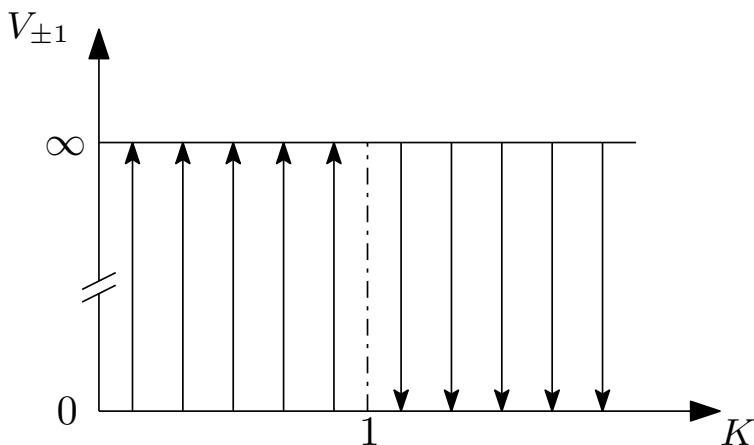
Figure 4.1: A schematic plot of the global RG flow of Kane-Fisher renormalization. Note $V_{\pm 1} = \infty$ corresponds to $t = 0$.

becomes relevant whenever $K < 1$, driving the system to isolated LL pieces (an insulator). Otherwise, if $K > 1$, the perturbation is always irrelevant, and the system remains a perfect LL (a superfluid).

4.4 Instanton theory

It turns out all the SF-I transitions described in the previous two sections can be understood from properties of 1D Popov's hydrodynamic action [47]. In one dimension, the topological term of Popov's hydrodynamic action Eq. (1.21) acquires the following form,

$$\int dx \int_0^{\beta\hbar} d\tau \, in_0(x)\partial_\tau\phi(x,\tau) = \sum_\nu 2\pi ip_\nu \int_{x_{\nu_-}}^{x_{\nu_+}} dx \, n_0(x) \equiv \sum_\nu 2\pi ip_\nu\gamma(x_{\nu_-},x_{\nu_+}), \quad (4.34)$$

where $\sum_\nu$ is the summation over all the vortex–anti-vortex pairs in the two-dimensional phase field $\phi(x,\tau)$, p_v is the charge of the vortex–anti-vortex pair ν, $x_{\nu_-}(x_{\nu_+})$ is the position of the the vortex (anti-vortex), and $\gamma(x_{\nu_-},x_{\nu_+}) = \int_{x_{\nu_-}}^{x_{\nu_+}} n_0(x)\,dx$. In the path integral language of time evolution in the imaginary time, these vortices (anti-vortices) correspond to instantons (anti-instantons) where the phase undergoes a rapid change of $2\pi p_\nu$, making a minimal contribution to the action [66, 67].

Without the topological term, the 1D SF-I transition is driven by the proliferation of vortex–anti-vortex pairs in the two-dimensional phase field $\phi(x,\tau)$ where the BKT theory provides an adequate description. With this term, the physics of 1D SF-I transition is still very similar to the BKT physics since it only limits the type of vortices and anti-vortices that can make a non-zero contribution to the partition function. For MI-SF transitions in pure systems with integer fillings, $n_0(x)$ is a position independent integer, and all types of vortices and anti-vortices are allowed. The partition function in the two-dimensional phase field is thus identical to that of the continuum limit of two-dimensional (2D) XY model, and the critical condition is $K_c = 2$ with dynamical critical exponent $z = 1$. In generic disordered systems, due to the randomness in $n_0(x)$, the disorder average of $e^{2\pi ip_\nu\gamma(x_{\nu_-},x_{\nu_+})}$, denoted as $f(x_{\nu_+} - x_{\nu_-})$, decays over microscopic length scales. At large length scale, $f(x)$ can be replaced with $\delta(x)$. The effect of disorder is, therefore, to impose the condition that only vertical vortex–anti-vortex pairs can contribute to the partition function. From the standard free-energy-sign argument [48], the critical condition is then given by $K_c = 3/2$ since the degree of freedom of a pair of vortexes in the system is reduced from four to three. In this way, we recovered the Giamarchi–Schulz critical condition and showed that the critical condition is valid beyond the weak disorder limit. For a single impurity, $f(x_{\nu_+} - x_{\nu_-})$ is zero unless x_{ν_-} and x_{ν_+} are centered around the impurity point $x = 0$ (the imaginary time

position of the vortex and the anti-vortex is arbitrary). This leads to the critical condition $K_c = 2/2 = 1$, in agreement with Kane-Fisher physics.

4.5 Asymptotically exact theory of superfluid–Bose-glass quantum phase transition in one dimension

The general discussion based on Popov's hydrodynamic action seems to imply that proliferation of instanton–anti-instantons is the only mechanism of zero-temperature SF-I in a generic 1D disordered boson system. However, the previous discussion implicitly assumes that starting from certain mesoscopic length scale the full system can be treated as a whole LL. This is not *a priori* true for strong disorder where, at mesoscopic length scales, the system is best viewed as superfluid lakes separated by weak links (tunnel junctions). It is tempting to assert that although weak links play a role in renormalizing the LL parameter, the transition is still driven by the proliferation of instanton–anti-instantons, and that from Kane-Fisher physics weak links are irrelevant because $K_c \geq 3/2$. However, this claim is also incorrect because of a subtle difference here: the bare strength of the typical weakest link becomes ever weaker with increasing system size, while in Kane-Fisher physics the bare strength of the single weak link is fixed. With the renormalization effect of the LL parameter by hydrodynamic phonons taken into consideration (Kane-Fisher physics), a careful study of the role of the typical weakest links reveals a new mechanism of SF-I transition driven by weak links in one dimension. This new weak-link universality class is named "scratched-XY criticality" (sXY) because, in the 2D classical system, the transition becomes the SF-NL transition of a XY model with column disorder in the form of parallel "scratches". While for weak disorder the mechanism of proliferation of vortex–anti-vortex always preempts the weak-link mechanism, the situation is different in the strong disorder regime. In this section, we closely follow [58] to present the new theory and study the sXY criticality.

4.5.1 Distribution of weakest links

To explore the possible effect of weak links in driving the SF-I phase transition, we need to characterize the distribution of weak links first. Theories addressing such links typically assume a strong power-law distribution for a typical weakest link in a system of length L as

$$J_0^{(L)} \propto \frac{1}{L^{1-\zeta}}, \tag{4.35}$$

where $J_0^{(L)}$ can be thought of as a Josephson coupling over the weak link, and ζ is a well-defined, irrenormalizable microscopic property of the disordered model. Equation (4.35) can be justified microscopically in a number of situations [68], and, in particular, for the classical-field counterpart of the model (1.7).

We postulate that (4.35) is valid for our quantum case. Specifically, the building blocks of the RG theory are patches of LL separated by sharply defined weak links, the nature of the latter being qualitatively similar to weak links in the classical-field system. By "sharp" we mean the absence of logarithmic corrections to the power law distribution, irrespective of weak-link properties (*e.g.*, such as its size). Under these assumptions, the above-mentioned classical-field phase transition [68] happens at $\zeta = 0$. We will verify in subsection 4.5.5 that (4.35) indeed holds numerically in all relevant regimes of the Bose-Hubbard model.

While it is difficult to rigorously derive (4.35) for the model (1.7), we can still argue why one should expect this law (the so called exponentially rare–exponentially weak consideration). Introduce the *typical length*, $r^{(L)}$, of the weakest link in the system of size L. In the model (1.7) and similar systems, the weakest link is nothing but a rare disorder realization such that within the length $r^{(L)}$ we have a mesoscopic piece of an insulating state. With respect to its local superfluid environment, this piece behaves as a Josephson junction,

$$J_0^{(L)} \propto e^{-c_2 r^{(L)}}, \tag{4.36}$$

with a certain well-defined (in the limit of $r^{(L)} \to \infty$ and $L \to \infty$) parameter $c_2 > 0$.

Note that $r^{(L)}$ in (4.36) is a sharply defined quantity, since its absolute uncertainty, of the order of some microscopic length, significantly changes the value of $J_0^{(L)}$. With this fact in mind, we write the condition for the link in question to happen with a probability of order one as

$$L\,e^{-c_1 r^{(L)}} \sim \text{const}.$$ (4.37)

The exponential factor, with a certain parameter $c_1 > 0$, is justified by the natural requirement that the disorder correlation radius is much smaller than $r^{(L)}$. The factor L takes into account the number of independent realizations (translations) of the rare region. From (4.37) we have $r^{(L)} = (1/c_1) \ln L + \mathcal{O}(1)$. Substituting this into (4.36) yields (4.35), with $\zeta = 1 - c_2/c_1$.

4.5.2 Kane–Fisher renormalization of the weakest links

As has been discussed before, the coupling across a link of strength J_0 is described by the term

$$J_0 \int d\tau \, \cos[\phi_+(\tau) - \phi_-(\tau)],$$ (4.38)

to be added to Popov's hydrodynamic action with $\phi_\pm$ being the phase field just before and after the link. The link is considered weak if the condition

$$J_0 \lambda_0 \kappa \ll 1$$ (4.39)

is met at the microscopic cutoff scale λ_0, and the RG equation for the scale-dependent strength of weak link, $J(\lambda)$, is (here we do not rescale space for later convenience)

$$\frac{dJ(\lambda)}{d\ln\lambda} = -\frac{1}{K(\lambda)}J(\lambda).$$ (4.40)

The condition (4.39) can be arrived from the following consideration. The link is perturbative if the number of particles in each of the two systems is a good quantum number despite the presence of the link. Speaking in the "Coulomb-blockade" language, this requires that J_0 be much smaller than the charging energy. Recalling that the latter is $\sim 1/(\kappa\lambda_0)$, we get (4.39).

For the sXY-criticality to occur, the critical LL parameter must be $K_c \geq 3/2$, meaning that while the absolute strength of the link, $J(\lambda)$, decreases under the RG flow, its relative strength $J\lambda\kappa$ increases. Hence, the renormalization of J inevitably stops at the *clutch scale* λ_* given by

$$J(\lambda_*)\lambda_*\kappa \sim 1 \,, \tag{4.41}$$

where perturbation theory is no longer valid. Therefore, upon completing the Kane-Fisher renormalization at the clutch scale λ_*, the link (4.35) picks up a certain renormalization factor $f(\lambda_*)$. With the help of the integral form of (4.40) this factor can be expressed as

$$f(\lambda_*) = \exp\left[-\int_0^{\ln\lambda_*} \frac{d\ell}{K(\ell)}\right]\,, \qquad \ell = \ln(\lambda/\lambda_0)\,. \tag{4.42}$$

The clutch condition (4.41) yields the following relation between λ_* and the microscopic strength of the weak link (below $J_0 \equiv J_0^{(L)}$)

$$J_0 f(\lambda_*)\lambda_*\kappa \sim 1\,. \tag{4.43}$$

Finally, the renormalization of the superfluid stiffness by the weakest link, $J_* = J_0 f(\lambda_*)$, in the system of size $\sim L$ obeys the flow equation

$$\frac{d\Lambda^{-1}}{d\ell} \sim \frac{1}{J_* L} \sim \frac{1}{J_0 f(\lambda_*)\,L} \sim \kappa\frac{\lambda_*}{L}\,. \tag{4.44}$$

To avoid potential problems with the tail of the distribution of (abnormally) weak links, we understand $\Lambda^{-1}(\ell)$ as the median value for different disorder realizations at a given system

size. The theorem of critical self-averaging [56] allows us to deal with the median value rather than the whole distribution.

Since κ does not flow with ℓ, we readily rewrite (4.44) as the flow equation for K

$$\frac{dK}{d\ell} = -wK^3 , \tag{4.45}$$

where

$$w \sim \lambda_*/L \equiv e^{\ell_* - \ell} , \tag{4.46}$$

and $\ell_* = \ln(\lambda_*/\lambda_0)$, $\ell = \ln(L/\lambda_0)$. Along with $K(\ell)$, the function $w(\ell)$ (characterizing the role of weak links at a given ℓ) plays a central role in the flow equations. The controllability of the RG theory requires that $dK(\ell)/d\ell \ll K(\ell)$ [*i.e.*, $K(\ell)$ flows slowly along the scales of distance], which translates into

$$w(\ell)K^2(\ell) \ll 1 . \tag{4.47}$$

Below we will see that this requirement is consistent with the flow equations since the latter guarantee $\lim_{\ell \to \infty} w(\ell) = 0$ in the superfluid phase, including the critical point.

To obtain the flow equation for $w(\ell)$, we substitute J_0 of (4.35) into (4.43),

$$\frac{\lambda_*}{L^{1-\zeta}} f(\lambda_*) = \text{const} . \tag{4.48}$$

Taking the logarithm on both sides and differentiating with respect to ℓ using (4.42),

$$\frac{d\ell_*(\ell)}{d\ell} = \frac{1 - \zeta}{1 - K^{-1}(\ell_*)} . \tag{4.49}$$

Differentiating the definition (4.46) with respect to ℓ and using (4.49), we get

$$\frac{dw}{d\ell} = \frac{1 - \zeta K(\ell_*)}{K(\ell_*) - 1} w . \tag{4.50}$$

Up to higher-order corrections, we can replace $K(\ell_*)$ with $K(\ell)$ in the r.h.s. of (4.50). Indeed, Taylor expanding $K(\ell_*)$ with (4.45) and (4.46) taken into account, we have

$$K(\ell_*) = K(\ell) + wK^3(\ell)(\ell - \ell_*) + \cdots$$
$$= K(\ell) + K^3(\ell)w\ln w^{-1} + \cdots, \tag{4.51}$$

so that,when writing $K(\ell) = \zeta^{-1} + x(\ell)$, the r.h.s. of (4.50) becomes

$$\frac{1 - \zeta K(\ell_*)}{K(\ell_*) - 1}\, w = -\frac{\zeta[x(\ell) + K^3(\ell)w\ln w^{-1} + \cdots]}{K(\ell) + K^3(\ell)w\ln w^{-1} - 1 + \cdots}\, w\,. \tag{4.52}$$

Replacing $K(\ell_*)$ with $K(\ell)$ is legitimate if $K^3(\ell)w\ln w^{-1} \ll x(\ell)$. For large enough ℓ, this condition is always satisfied. As we will see later [from (4.76) and (4.77)], even in the worst case scenario, $i.e.$ at the critical point when the asymptotic flow of K is the strongest and $x(\ell) \to 0$, we have

$$K^3 w\ln w^{-1} \propto \frac{1}{\zeta^2\ell^2}\ln\frac{\ell}{\sqrt{\zeta}} \ll \frac{1}{\zeta^2\ell} \sim x(\ell). \tag{4.53}$$

Finally, taking the renormalization of K by instanton–anti-instanton pairs into consideration brings us to three coupled RG equations

$$\frac{dy}{d\ell} = (3/2 - K)\,y\,, \tag{4.54}$$

$$\frac{dK}{d\ell} = -K^2y^2 - K^3w\,, \tag{4.55}$$

$$\frac{dw}{d\ell} = \frac{1 - \zeta K}{K - 1}\, w\,. \tag{4.56}$$

Equation (4.54) is the standard Kosterlitz–Thouless equation for the flow of the vortex fugacity y, except that the coefficient in front of y is $(3/2 - K)$ instead of $(2 - K)$. This is because in the $(1 + 1)$D representation of the 1D disordered system only vertical vortex–anti-vortex pairs contribute to the renormalization of the superfluid density [47]. Equation

55

(4.55) describes the renormalization of the LL parameter by the instanton–anti-instanton term y^2 and by the weak-link term w. Finally, equation (4.56) is the same as (4.50), with the above-discussed replacement $K(\ell_*) \to K(\ell)$.

Once the RG flow hits the point $K(L) = \max\{3/2, \zeta^{-1}\}$, it quickly flows to an insulating state, $K(\infty) = 0$. We thus identify two different universality classes: (i) the GS universality class with the universal critical value of the LL parameter $K_c = 3/2$, and (ii) the sXY universality class, where the critical LL parameter is semi-universal, $K_c = \zeta^{-1}$.

4.5.3 Physics in the weak-link regime

In this section, we study the critical behavior in the weak-link regime where the phase transition to the insulating phase is driven by the weakest links whereas proliferation of instanton–anti-instanton pairs remains irrelevant. Explicit solutions to the flow equations are obtained to demonstrate the BKT-like nature of the criticality. Equation (4.44) takes into account only the contributions of *microscopic* weakest links. We justify this crucial assumption by showing that the contribution of *composite* weak links is always subdominant.

4.5.3.1 Criticality driven by the weakest links

We define the weak-link regime by the requirement $\zeta < 2/3$ so that the criticality is due to the weakest links. To study this critical behavior we neglect the instanton–anti-instanton pair term y^2 in (4.55) and the relevant RG equations simplify to

$$\frac{dK}{d\ell} = -K^3 w \,, \tag{4.57}$$

$$\frac{dw}{d\ell} = \frac{1/\zeta - K}{(K-1)/\zeta} \, w \,. \tag{4.58}$$

The first integral is found by dividing (4.58) through (4.57),

$$dw = \frac{\zeta K - 1}{(K-1)K^3} dK \,, \tag{4.59}$$

56

and then integrating both sides of the equation. It reads

$$w = A - f(\zeta, K), \tag{4.60}$$

where A is an integration constant depending on the microscopic parameters and

$$f(\zeta, K) = \frac{1}{2K^2} + \frac{1 - \zeta}{K} + (1 - \zeta)\ln\frac{K - 1}{K}. \tag{4.61}$$

Since on approach to the critical point from the superfluid phase $w(\ell = \infty) = 0$, the integration constant A satisfies

$$A = f(\zeta, K(\ell = \infty)) \tag{4.62}$$

in the superfluid phase and at the critical point. In our model (1.7), $A = A(U, \Delta)$. Let us follow the parameter A along a line segment in the plane (U, Δ). Parameterizing the segment as $U = U(t)$, $\Delta = \Delta(t)$, with a certain parameter t, and assuming that the segment crosses the SF-BG critical line at the point (U_c, Δ_c), in the vicinity of the point $(U_c, \Delta_c) \equiv (U(t_c), \Delta(t_c))$ we have:

$$A(t) \approx A(t_c) + A_1(t_c - t). \tag{4.63}$$

Similarly, following ζ on the same line segment we have

$$\zeta(t) \approx \zeta(t_c) + A_2(t_c - t). \tag{4.64}$$

Here A_1 and A_2 are certain constants, t_c is the critical value of t. Without loss of generality, we assume $t < t_c$ in the superfluid phase. Substituting (4.63) and (4.64) into (4.62) and keeping only the leading terms, we get

$$K_\infty(t) - \zeta^{-1}(t_c) \propto \sqrt{t_c - t}. \tag{4.65}$$

Hence, the LL parameter in the scratched-XY universality class demonstrates the same square-root cusp as in the conventional BKT case. The analogy with BKT transition can be traced further by investigating the linearized flow equations near the critical point:

$$\frac{d\tilde{w}}{d\ell} = -2\tilde{x}\tilde{w}\,, \tag{4.66}$$

$$\frac{d\tilde{x}}{d\ell} = -\tilde{w}\,. \tag{4.67}$$

Here we first introduce $x(\ell)$ such that $K(\ell) = \zeta_c^{-1} + x(\ell)$, and then rescale x and w:

$$\tilde{x}(\ell) = \frac{\zeta_c^2 \, x(\ell)}{2(1 - \zeta_c)}\,, \tag{4.68}$$

$$\tilde{w}(\ell) = \frac{w(\ell)}{2(1 - \zeta_c)\zeta_c}\,. \tag{4.69}$$

The first integral of the system (4.66)–(4.67) is readily found:

$$\tilde{w}(\ell) = \tilde{x}^2(\ell) - \tilde{A}\,. \tag{4.70}$$

Here $\tilde{A}$ is an integration constant. By definition, $\tilde{A}$ vanishes at the critical point. The constant $\tilde{A}$ is an analytic function of the microscopic parameters, because (4.70) is valid for *finite* ℓ where both $\tilde{x}(\ell)$ and $\tilde{w}(\ell)$ cannot have singularities. This enables us to expand $\tilde{A}$ as

$$\tilde{A} \approx B(t_c - t)\,, \tag{4.71}$$

with a positive constant B.

The form of the complete solutions depends on the sign of $\tilde{A}$. For the superfluid side $(\tilde{A} > 0)$, we have:

$$x(\ell) = \frac{2(1 - \zeta_c)}{\zeta_c^2} \frac{\sqrt{\tilde{A}}}{\tanh\left[\sqrt{\tilde{A}}\,(\ell - \ell_0)\right]}, \tag{4.72}$$

$$w(\ell) = \frac{2(1 - \zeta_c)\zeta_c\tilde{A}}{\sinh^2\left[\sqrt{\tilde{A}}\,(\ell - \ell_0)\right]}. \tag{4.73}$$

For the insulator side $(\tilde{A} < 0)$, the solution is:

$$x(\ell) = \frac{2(1 - \zeta_c)}{\zeta_c^2} \frac{\sqrt{|\tilde{A}|}}{\tan\left[\sqrt{|\tilde{A}|}\,(\ell - \ell_0)\right]}, \tag{4.74}$$

$$w(\ell) = \frac{2(1 - \zeta_c)\zeta_c|\tilde{A}|}{\sin^2\left[\sqrt{|\tilde{A}|}\,(\ell - \ell_0)\right]}. \tag{4.75}$$

At the critical point, we have

$$x(\ell) = \frac{2(1 - \zeta_c)}{\zeta_c^2} \frac{1}{\ell - \ell_0}, \tag{4.76}$$

$$w(\ell) = \frac{2(1 - \zeta_c)\zeta_c}{(\ell - \ell_0)^2}. \tag{4.77}$$

The second integration constant ℓ_0 has a trivial meaning of the logarithm of the length unit. The correlation length ξ hence diverges near the critical point in the same characteristic way as in the conventional BKT case: $\ln \xi \sim 1/\sqrt{|\tilde{A}|} \sim 1/\sqrt{|t_c - t|}$.

4.5.3.2   Irrelevance of composite weak links

To make sure that the theory of the sXY universality is fully consistent, it is important to demonstrate that *composite* weak links play only a subdominant role (in contrast to

59

the assumptions of [51–53]) and thus can safely be ignored in the RG analysis. Consider the simplest composite weak link—to be referred as a d-pair for brevity—formed by two microscopic weak links (of comparable microscopic strength J_0) separated by a distance d much larger than the microscopic scale but much smaller than the clutch scale for any of the two links. Up to the length scale $\lambda \sim d$, the Kane–Fisher renormalization of the two links takes place independently and reduces to multiplying each of the two J_0's by the factor

$$f(d) = \exp\left[-\int_0^{\ln d} \frac{d\ell}{K(\ell)}\right],\tag{4.78}$$

Mathematically, the merger of two renormalized links of strength $J_1(d) \sim J_2(d) \sim J_0 f(d)$ into one composite link takes place upon integrating out the phase field between the two links. [We note in passing that, in the renormalized theory, the phase field between the links depends only on τ and not on x.] An explicit calculation yields the following estimate for the effective strength of the composite link

$$J_{\text{comp}}^{(d)} \sim J_1(d)J_2(d)\kappa d.\tag{4.79}$$

This estimate is physically transparent, and immediately follows from second-order perturbation theory by considering the d-pair as a quantum dot in the "Coulomb blockade" regime. Then, $J_1(d)$ and $J_2(d)$ are two effective single-particle tunneling matrix elements and $1/(\kappa d)$ is the charging energy of the dot. For length scales $\lambda > d$ the Kane–Fisher renormalization of the composite link reduces to multiplying (4.79) by the factor

$$\exp\left[-\int_{\ln d}^{\ln \lambda} \frac{d\ell}{K(\ell)}\right] = f(\lambda)/f(d).\tag{4.80}$$

Hence, for the renormalized strength of a d-pair we have

$$J_{\text{comp}}^{(d)}(\lambda) = \kappa d J_0^2 f(d)f(\lambda) \qquad (\lambda > d).\tag{4.81}$$

60

The clutch scale for the d-pair, $\lambda_*^{(d)}$, then follows from the condition $J_{\text{comp}}^{(d)}(\lambda)\lambda_*^{(d)} \sim 1$ (in units $\kappa = 1$)

$$J_0^2 f(d) f(\lambda_*^{(d)}) \lambda_*^{(d)} d \sim 1 \,. \tag{4.82}$$

This is all we need to compare the contribution of d-pairs with the one of isolated weak links.

For a given system size L and scale d we only need to account for those d-pairs which occur with a probability of order one because pairs with higher density are absorbed into the renormalized value of $\Lambda_s(L)$ whereas unlikely pairs are accounted for at larger system sizes. This defines the characteristic J_0 as a function of L and scale d:

$$\left[J_0^{1/(1-\zeta)} \right]^2 d = 1/L \tag{4.83}$$

for d-pairs within the scale d. For an explicit calculation, we confine ourselves to the critical point, which is the most dangerous regime for the putative relevance of composite weak links. Here, with (4.76) we have

$$f(\lambda) = \lambda^{-\zeta} \ln^{2(1-\zeta)}(\lambda) \qquad \text{(critical flow)} \,. \tag{4.84}$$

Combining (4.82) and (4.83) with (4.84), we obtain

$$\left[\ln^2(d) \ln^2(\lambda_*^{(d)}) \frac{\lambda_*^{(d)}}{L} \right]^{1-\zeta} \sim 1 \,. \tag{4.85}$$

Finally, replacing $\lambda_*^{(d)}$ with L under the logarithm, we get (with logarithmic accuracy)

$$\frac{\lambda_*^{(d)}}{\lambda} \sim \frac{1}{\ln^2 d \, \ln^2 L} \,, \tag{4.86}$$

and observe that the contribution of large d-pairs to the renormalization of Λ is suppressed relative to (4.77) by a factor of $\ln^{-2}(d)$. Most importantly, the integral over the pair scales

$\int d[\ln d]$—yielding the total renormalization contribution of all relevant d-pairs—converges at the *lower* limit, where microscopic pairs (and other multi-link complexes) are an integral part of the original exponentially-rare exponentially-weak distribution of single links.

4.5.4 Interplay between weak-link and Giamarchi–Schulz scenarios

The next natural question to ask is how the well-known GS criticality based on proliferation of instanton–anti-instanton pairs crosses over to the weak-link criticality. It turns out that weak links are more aggressive and the instanton–anti-instanton pairs can be neglected in the asymptotic flow at the multicritical point. A direct consequence of this fact is the continuous first-order derivative of the transition line at the multicritical point.

4.5.4.1 RG equations for small deviations from the multicritical point

To study the competition between weak links and instanton–anti-instanton pairs in the vicinity of the multicritical point, we rewrite identically $K(\ell) = 3/2 + x(\ell)$, $\zeta = 2/3 + \delta$, and consider $x > 0$ and δ as small parameters to simplify the RG equations. The multicritical point is fixed by $\delta = 0$ with positive/negative δ corresponding to the GS/sXY criticality, respectively. Expanding (4.54), (4.55) and (4.56) to leading order in x and δ results in

$$\frac{dy}{d\ell} = -xy\,, \tag{4.87}$$

$$\frac{dx}{d\ell} = -y^2 - w\,, \tag{4.88}$$

$$\frac{dw}{d\ell} = -\left(\frac{4}{3}x + 3\delta\right)w\,. \tag{4.89}$$

Here functions y and w were rescaled to eliminate multiplicative constants. This is a set of three coupled, first-order differential equations, implying that the solution will have three free constants. One of them, ℓ_0, has the same meaning as in subsec. 4.5.3 [see (4.72)–(4.77)]. Assuming corresponding choice of length units, we set $\ell_0 = 0$ from now on. The other two

62

integration constants, denoted as C and D below, are related to the microscopic parameters of the system and dictate the location of the SF-BG transition.

Extracting x from (4.87) and plugging it into (4.89) leaves us with

$$\frac{d \ln w}{d\ell} + 3\delta = \frac{4}{3} \frac{d \ln y}{d\ell} . \tag{4.90}$$

Integrating both sides over ℓ leads to the first integral

$$y^2 = \frac{1}{C^{3/2}} w^{3/2} e^{9\delta\ell/2} . \tag{4.91}$$

In the weak-link regime, and at the multicritical point, where $\delta \leq 0$, (4.91) implies $y^2 \ll w$; i.e., starting from some mesoscopic length scale the weak-link term dominates over the instanton–anti-instanton pairs. The 3δ in (4.89) results in a non-universal critical parameter $K_c > 3/2$ since otherwise w diverges. In the GS regime, the flow starts with $y^2 \ll w$ but ultimately crosses over to $y^2 \gg w$ at some length scale $\tilde{\ell}$ (see below) leading to a universal critical LL parameter $K_c = 3/2$ and the familiar BKT critical behavior.

Dividing (4.88) by (4.89) and making use of (4.91), we have

$$(4x/3 + 3\delta) \, dx = \left(C^{-3/2} w^{1/2} e^{9\delta\ell/2} + 1 \right) dw . \tag{4.92}$$

Integrating both sides from ℓ_0 to ℓ and utilizing the *second mean value theorem for definite integrals* results in

$$\left(x + \frac{9}{4}\delta \right)^2 = \left(\frac{w}{C} \right)^{3/2} e^{9\delta\eta\ell/2} + \frac{3w}{2} + D , \tag{4.93}$$

where $0 < \eta < 1$ and D is our last integration constant.

The meaning of the integration constant D is easily revealed by examining the weak-link critical line where $K_c(\infty) = \zeta^{-1} = 3/2 - 9\,\delta/4$ and $x_c(\infty) = -9\,\delta/4$ up to leading order in δ. From (4.93) the weak-link critical line corresponds to

$$D_c = 0. \tag{4.94}$$

Since δ is a microscopic parameter, one can use δ and D (controlling the location of the multicritical point and the transition line, respectively) to conveniently parameterize the whole problem.

4.5.4.2 Giamarchi–Schulz regime and the parabolic crossover

In the GS regime the critical condition $K_c = 2/3$ translates into $x_c(\infty) = 0$. Moreover, the GS critical line will lie on the positive side of the $D = 0$ line extended beyond the multicritical point (see also below). However, as can be seen from (4.91), the crossover length scale for the dominance of the vortex fugacity term satisfies the condition $\tilde{\ell} > 1/\delta$, meaning that at small δ (i) the initial flow of K is due to weak links, and (ii) the critical line is closely following the $D = 0$ line. Indeed, substituting (4.91) into (4.93) gives

$$\left(x + \frac{9}{4}\delta\right)^2 = y^2 e^{-(1-\eta)\delta\ell} + \frac{3w}{2} + D. \tag{4.95}$$

The condition for the Giamarchi–Schulz critical line is then just

$$D_c = (9\delta/4)^2 = \frac{81}{16}\delta^2\,, \tag{4.96}$$

since the first and second terms on the r.h.s flow to zero.

For the 1D disordered Bose-Hubbard model the microscopic parameter ζ (and thus δ) and the integration constant D are supposed to be analytic functions of the model parameters

U and Δ. Since (4.96) predicts that the SF-BG boundary has a continuous first derivative across the multicritical point in the (D, ζ)-plane, the same property holds in the (U, Δ)-plane. By the same token the second derivative is discontinuous. Therefore, the crossover is *parabolic* in the (U, Δ)-plane.

4.5.5 Ground-state phase diagram of the one-dimensional disordered Bose-Hubbard model

4.5.5.1 Protocol of extracting ζ

Our numerical procedure of extracting ζ is based on measuring small probabilities, $P \propto J_0^{1/(1-\zeta)}$, of *rare realizations* of disorder, when in a system of (moderate) size L there is an anomalously weak link, J_0, with the clutch scale much larger than the system size: $\kappa J(L) L \ll 1$. [Here $J(L) \equiv J(\lambda = L)$.] With open boundary conditions such a link would cut the system into two essentially independent pieces. With twisted boundary conditions it acts as a Josephson junction in a superfluid ring: the particle flux (persistent current) in the ring, j, in response to a phase twist, φ, is related to $J(L)$ by

$$j = \frac{\partial F}{\partial \varphi} = J(L) \sin \varphi \qquad (T \ll 2\pi^2 \Lambda/L), \qquad (4.97)$$

where F is the free energy. The first equality in (4.97) is absolutely general and does not imply any extra condition. A delicate aspect of the static thermodynamic response to the gauge phase in low-dimensional systems is the necessity to address the contribution of supercurrent states (*i.e.*, states with non-zero global winding numbers of the phase field around the ring) [69]. Supercurrent states can dramatically affect the second equality in (4.97) at elevated temperature: In order to guarantee that their contribution is negligible, we need to consider temperatures much lower than the energy of the first supercurrent state, $T \ll 2\pi^2 \Lambda/L$.

With (4.97) one relates $J(L)$ to the second derivative of F with respect to φ at $\varphi = 0$:

$$J(L) = \left.\frac{\partial^2 F}{\partial \varphi^2}\right|_{\varphi=0} . \qquad (4.98)$$

Within the worldline representation (used in our numerical simulations by the worm algorithm), the r.h.s. of (4.98) is readily obtained by the well-known Pollock–Ceperley formula [31]

$$\left.\frac{\partial^2 F}{\partial \varphi^2}\right|_{\varphi=0} = T \left\langle M^2 \right\rangle\big|_{\varphi=0} , \qquad (4.99)$$

expressing the linear response as the variance of the worldline winding number M at a given temperature T at $\varphi = 0$.

The measured strength $J(L)$ of the anomalously weak link is, of course, different from the microscopic value J_0 due to Kane–Fisher renormalization $(\lambda_0/L)^{1/K}$. However, this renormalization does not depend on J_0, and cannot affect the power-law exponent ζ. Hence,

$$J_0 \propto T \left\langle M^2 \right\rangle\big|_{\varphi=0} \qquad (4.100)$$

for all weak links at given L and T. Furthermore, for purposes of extracting ζ, (4.100) can be used even at an elevated temperature $T > 2\pi\Lambda/L$ when the persistent current response (4.97) is dramatically renormalized (suppressed) by the supercurrent states [69]. Indeed, in view of the perturbative nature of the weak link response, both Kane–Fisher and supercurrent renormalizations reduce to a certain factor $\tilde{f}(L,T)$ independent of J_0. In terms of J_0 and $\tilde{f}(L,T)$, we then have

$$J_0 \, \tilde{f}(L,T) = T \left\langle M^2 \right\rangle\big|_{\varphi=0} , \qquad (4.101)$$

justifying (4.100).

If the concept of irrenormalizable weak links is correct, then finding the weakest link among the $N \gg 1$ different disorder realizations in a system of a moderate size L is equivalent

to doing the same in a much larger single system of size $L_1 = LN$. This leads to an efficient protocol for determining ζ using the approach by varying N (and L, to validate the concept). The three natural limitations on L and N are: (i) L has to be sufficiently large to capture all the essential microscopic physics of weak links; (ii) N should not be "astronomically" large to ensure that the size of the typical weakest link remains much smaller than L. In practice, this condition is hard to violate even for a moderate value of $L = 20$; (iii) N should be large enough to ensure that the clutch scale of the weakest link in a system of size L exceeds L.

To extract ζ, we simulate $N_i L = [10e^i]$ $(i = 1, 2, 3, \dots)$ different disorder realizations (here $[\dots]$ stands for the closest integer) and record the smallest weak link parameter J_i in a given simulation run; $i.e.$, we use an equidistant mesh for $\ln NL$ to probe different length scales. To suppress statistical noise, the procedure is repeated $R = 20, 30, 40$ times (depending on system size) and results from multiple runs, $J_i^{(k)}$ $(k = 1, 2, \dots, R)$, are used to determine the typical weak link value as an average over all runs, $J(N_i L) = \langle J_i^{(k)} \rangle_R$. Its error bar follows from the data dispersion, $\delta J(N_i L) = \sqrt{\{\langle [J_i^{(k)}]^2 \rangle_R - J^2(N_i L)\}/R}$. Finally, the data for $\ln J(NL)$ is fitted to a linear dependence

$$\ln J = (\zeta - 1) \ln NL + \text{const} , \tag{4.102}$$

to extract the power-law exponent ζ. A characteristic example of the ζ-analysis is shown in figure 4.2. We see that the data is perfectly described by a linear dependence, leading to an accurate determination of ζ. Within three-σ error margins, the slope of the linear fit does not change when going from $L = 20$ over $L = 30$ to $L = 40$. This behavior is in perfect agreement with the notion of ζ as an irrenormalizable microscopic parameter in the superfluid phase and in the critical region. In fact, figure 4.2 is representative of the worst-case scenario because according to our RG analysis (see figure 4.4 below) the parameter set

$(U = 4.2, \Delta = 3.8)$ belongs to the BG phase in close vicinity of the critical point when $L = 40$ is still smaller than the correlation length.
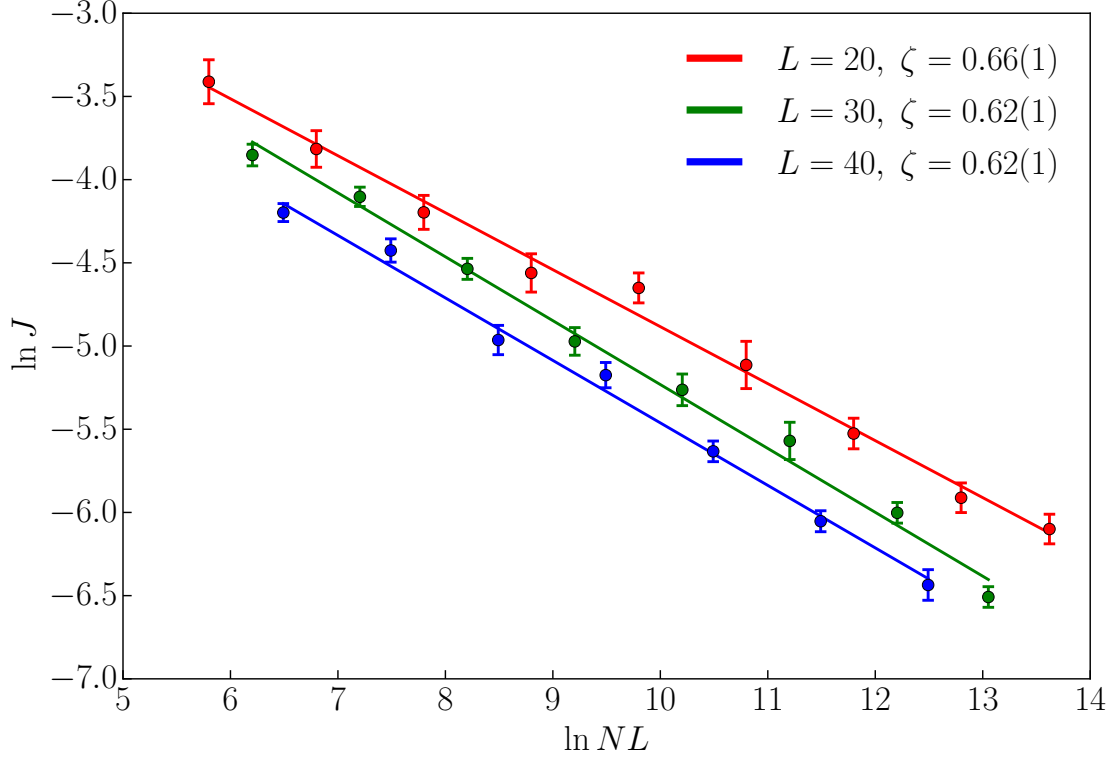
Figure 4.2: Determining ζ for $(U = 4.2, \Delta = 3.8)$ using (4.102). The error bars for ζ denote one standard deviation (deduced by the confidence level for a linear fit to all data points).

4.5.5.2 sXY critical line

In the weak-link regime we can neglect the instanton–anti-instanton effects in the asymptotic flow of the superfluid stiffness [*i.e.,* the term proportional to y^2 in (4.55)] in the SF phase and the critical region, and analyze the data using the simpler (4.60) with $A = f(\zeta, K(\infty))$ and

$$w = f(\zeta, K(\infty)) - f(\zeta, K) \,. \tag{4.103}$$

Since the $f(\zeta, x)$-function takes its maximum value at $x = 1/\zeta$, see (4.61), and the value of K can only decrease with the scale of distance, we immediately conclude that, if at some scale we have $K(L) > 1/\zeta$ and simultaneously $w(L) \leq f(\zeta, \zeta^{-1}) - f(\zeta, K(L))$, then the fixed point of the flow corresponds to $w(\infty) = 0$ and $K(\infty) \geq 1/\zeta$, *i.e.* the phase is superfluid. Otherwise, the flow reaches a point where $K(L') = 1/\zeta$ with $w(L') > 0$ and the flow continues to the BG phase.

To measure $K(L)$, we extract the compressibility $\kappa(L)$ and superfluid stiffness $\Lambda(L)$ from the particle number and winding number statistics. In the grand canonical ensemble the probability of finding a worldline configuration with a given N or W number is given by discrete Gaussian distributions

$$W_M(M) \propto e^{-LTM^2/2\Lambda} , \tag{4.104}$$

$$W_N(N) \propto e^{-(N-\bar{N})^2/2TL\kappa} , \tag{4.105}$$

where $\bar{N}$ is the average particle number. From this, the superfluid stiffness can be obtained as

$$\Lambda = LT \ln^{-1}\left[\frac{W_M^2(0)}{W_M(1)\,W_M(-1)}\right] , \tag{4.106}$$

and compressibility as

$$\kappa = \frac{1}{TL}\ln^{-1}\left[\frac{W_N^2([\bar{N}])}{W_N([\bar{N}]+1)\,W_N([\bar{N}]-1)}\right] , \tag{4.107}$$

where $[\bar{N}]$ is the closest integer to $\bar{N}$.

The protocol of determining the critical point is as follows. We fix the value of U and start with measuring the $\zeta(\Delta)$ dependence (all data points can be perfectly fit to a linear dependence). Next, we compute $K(L, \Delta)$ values for a number of different system sizes and Δ-points. $K(L, \Delta)$ is reported as the median of the distribution over several hundred (up to

69
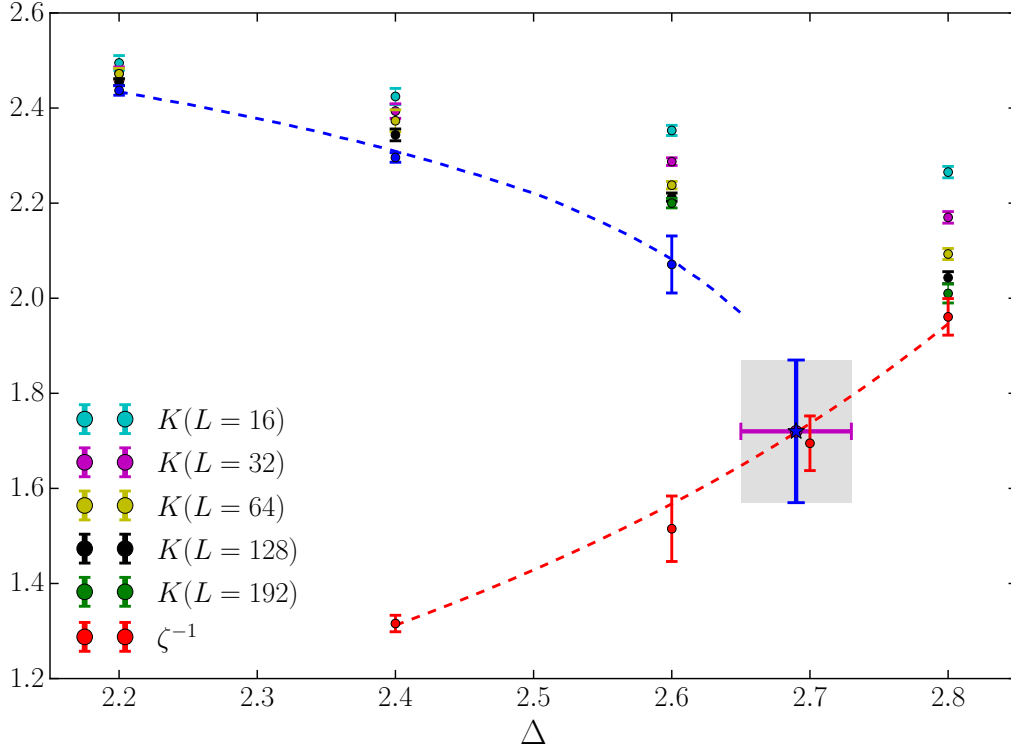
Figure 4.3: Fine-size (see the legend) and extrapolated values (blue points and dashed line) of the LL parameter K for different disorder strengths at $U = 2.5$. The red dashed line (with the red dots) is the $\zeta^{-1}(\Delta)$ function obtained by linear regression of the data for ζ. The SF-BG transition point is located within the Grey area where the phase is ambiguous from the fitting the RG flow due to uncertainties of $\zeta(\Delta)$ and $K(L, \Delta)$. We estimate the critical disorder strength to be at $\Delta_c(U) = 2.69(4)$ (the magenta point and half of the horizontal width of the Grey area); its error bar is relatively small thanks to the sharp square-root dependence of $K(\infty, \Delta)$. Correspondingly, the critical LL parameter is estimated to be $K_c(\infty) = 1.72 \pm 0.15$ (the blue star and half of the vertical width of the Grey area).

a thousand) disorder realizations. Finally, for each value of Δ, we employ (4.57) and (4.58) to extract the $w(L)$-function by fitting finite-size data to the flow equations. Depending on the result, we then either derive the thermodynamic limit answer for $K(\infty)$ from (4.103) or conclude that the flow is to the BG phase. To improve our estimate of the critical disorder strength, given a finite mesh in Δ, we interpolate $K(L, \Delta)$ data between the points using linear fits and proceed with the flow analysis as described above; higher-order polynomial fits produce similar results within the error bars. The critical parameter $\Delta_c(U)$ is then found from the intersection of $K(\infty, \Delta)$ and $\zeta^{-1}(\Delta)$ curves, see figure 4.3. Its error bar is mostly determined by the uncertainty on the closest ζ and $K(\infty)$ points.

4.5.5.3 Multicritical point and the Giamarchi–Schulz criticality

The multicritical point (U_*, Δ_*) separating the sXY and GS universality classes can be found from the intersection of the sXY critical and $\zeta = 2/3$ lines. Two circumstances help us to locate it relatively accurately. On the one hand, from the analysis performed in subsection 4.5.4 we conclude that the sXY critical line can be smoothly interpolated all the way to the intersection point. On the other hand, the sXY critical point $\Delta_C(U = 3.6) = 3.36$ [the black dot in figure 4.4] deduced by the protocol described in the previous subsection, landed on the $\zeta = 2/3$ line [located at $(U = 3.6,\ \Delta = 3.38)$] within error bars. This basically eliminates the need for determining the multicritical point from the intersection of interpolated curves. The procedure predicts

$$U_* = 3.40 \pm 0.23, \qquad \Delta_* = 3.25 \pm 0.15 . \tag{4.108}$$

The value for U_* is remarkably close to the critical value for the superfluid to Mott insulator transition in the absence of disorder.

By knowing the slopes of the sXY critical and $\zeta = 2/3$ lines in the (Δ, U)-plane and the location of the multicritical point, we are in a position to relate the integration constant
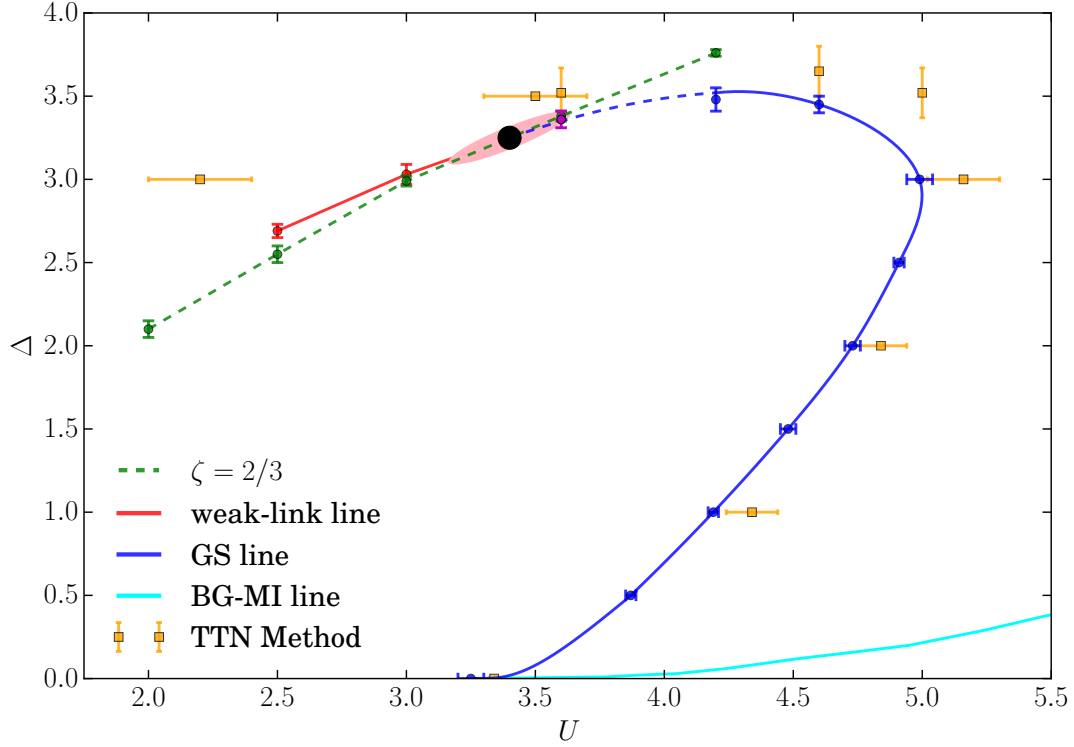
Figure 4.4: Ground-state phase diagram of the 1D disordered Bose-Hubbard model at unit filling factor. The sXY and GS critical lines are shown in red and blue, respectively. The intersection of the interpolated $\zeta = 2/3$ line (dashed green) with any of the other critical lines determines the multicritical point (black dot within the pink uncertainty region). The cyan line shows the gaps of the Mott insulator in the disorder-free system taken from [62], which signals the transition between the Mott insulator and the BG phase in the presence of disorder. We also show the $K(\infty) = 3/2$ line obtained by the Tree Tensor Network (TTN) method [70] (orange), which agrees with our GS-line within the error bars. As expected, in the weak-link regime, the TTN line ends inside the BG phase.

D and the small parameter δ, controlling the shape of the phase diagram in the vicinity of (U_*, Δ_*), to the Hamiltonian parameters. Using a linear expansion about the $D = 0$, $\delta = 0$ point

$$D = A_{11}(U - U_*) - A_{12}(\Delta - \Delta_*) \,, \tag{4.109}$$

$$\delta = A_{21}(U - U_*) - A_{22}(\Delta - \Delta_*) \,, \tag{4.110}$$

and numerical data determining the $D = 0$ and $\delta = 0$ curves, we find that

$$A_{11}/A_{12} = 0.55 \pm 0.11 \,, \qquad A_{21}/A_{22} = 0.65 \pm 0.06 \,. \tag{4.111}$$

Next, the dependence of $K(\infty)$ on Δ in the SF phase in the weak-link regime allows us to obtain A_{12}. Specifically, near the multicritical point (4.93) implies

$$K(\infty, \Delta) - 1/\zeta = \sqrt{D(\Delta)} \,, \tag{4.112}$$

This analysis allows us to determine the derivative of D with respect to Δ and results in

$$A_{12} = 1.0 \pm 0.2 \,. \tag{4.113}$$

Similarly, A_{22} controls the slope of the $\zeta(\Delta)$ line at fixed U. From the data sets computed at $U = 3.0$ and $U = 3.6$ and linearly extrapolated to the multicritical point, we find

$$A_{22} = 0.56 \pm 0.14 \,. \tag{4.114}$$

We are all set to make a quantitative prediction for the structure of the phase diagram in close vicinity of the multicritical point, including the location of the GS-line (the protocol

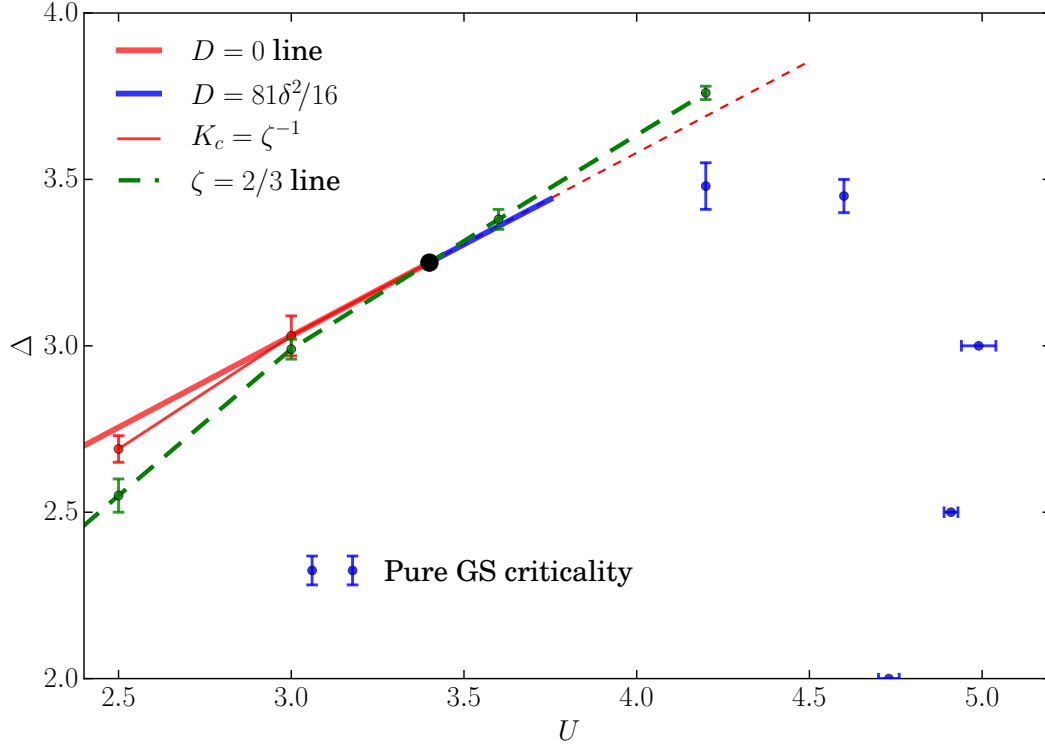Figure 4.5: The SF-BG phase diagram in the vicinity of the multicritical point. (4.109), (4.110), (4.111), (4.113), and (4.114) were used to plot the $D = 0$ (bold red and dashed red), $\delta = 0$ (dashed green), and $D = (81/16)\delta^2$ (bold blue) predictions for sXY, $\zeta = 2/3$, and GS lines, respectively. We also plot our numerical data for the same lines (same color scheme as in figure 4.4).

of calculating the GS line away from the multicritical point is outlined below). The result is shown in figure 4.5 where (4.109) and (4.110) are used to plot the $D = 0$, $\delta = 0$, and $D = (81/16)\delta^2$ [see (4.96)] curves for sXY, $\zeta = 2/3$, and GS lines, respectively. By observing reasonable agreement between this prediction and an independent calculation of the GS-line relatively far from the multicritical point we validate the proposed theory.

Deep in the GS regime, when the weak link term w in the RG equations can be neglected, we are back to the standard XY-universality class analysis. From

$$\frac{dy}{d\ell} = (3/2 - K)y \,, \tag{4.115}$$

$$\frac{dK}{d\ell} = -y^2 K^2 \,, \tag{4.116}$$

we readily obtain the first integral as

$$2\ln K + 3/K = y^2 + G \,, \tag{4.117}$$

where G is the integration constant. The thermodynamic state can be established by solving the RG flow just as we did for the weak-link regime. In the SF phase, the flow has a fixed point at $y = 0$ and $K(\infty) \geq 3/2$. Otherwise, if the finite-size system can reach a state with $K(L) = 3/2$ and $y > 0$, the flow will continue towards the BG phase with $K(\infty) = 0$. Numerically, we first fit the finite-size data to the RG flow to determine G and then use the above-mentioned property of the first integral (4.117) to determine the phase. Technically, this protocol is nearly identical to the one used in the weak-link regime and we do not repeat it here. The resulting GS-line is shown in figure 4.4.

4.5.6   Concluding remarks

The importance of our successful application of the sXY criticality theory to the SF-BG transition in model (1.7) is two-fold. First, we have corroborated the analytic theory of

the interplay between the two university classes and the structure of the phase diagram in the vicinity of the multicritical point. Second, we establish the qualitative and quantitative behavior of the ground-state phase diagram (and finite-size properties) of the Hamiltonian (1.7) numerically. The theory rests on a rather non-trivial postulate of the existence of an irrenormalizable power-law distribution of microscopic weak links. While being self-consistent—and, in this sense, rendering the theory asymptotically exact—the postulate can hardly be proven as a theorem. Therefore, the data in figure 4.2 demonstrating excellent agreement with the ζ-postulate is at least as important as the phase diagram shown in figure 4.4.

The ground-state phase diagram of (1.7) in the (U, Δ) plane features a characteristic line defined by the condition $\zeta(U, \Delta) = 2/3$. Strictly speaking, this line is well defined only in the superfluid phase and at the SF-BG phase boundary. However, the exponential divergence of the correlation length on approach to the SF-BG critical point guarantees that the $\zeta = 2/3$ line remains meaningful even inside the BG phase [see figure 4.4]; the data presented in figure 4.2 further illustrate this point. On the $\zeta < 2/3$ side from the $\zeta = 2/3$ line, the sXY criticality preempts the GS scenario. This, in particular, means that superfluidity with $3/2 < K(L) \leq 1/\zeta$ in this part of the phase diagram is guaranteed to be a finite-size effect, since the $L \to \infty$ phase is BG.

At the intersection of the $\zeta = 2/3$ line with the SF-BG phase boundary there is a multicritical point separating the GS and sXY criticalities. According to our analysis, the phase boundary remains smooth at the multicritical point but the curvature is discontinuous. For purely numeric reasons the angle between the $\zeta = 2/3$ line and the phase boundary happens to be rather small. As a result, despite accurately identifying the positions of both the $\zeta = 2/3$ line and the phase boundary, the uncertainty in the location of the multicritical point remains relatively large. Another consequence of the small angle intersection is that the critical value of K on the sXY line is only slightly higher than the GS value of $3/2$.

Under such circumstances, a brute-force observation of the violation of the GS scenario in the vicinity of the multicritical point becomes problematic (cf. [70]) even though our data in figure 4.3 are not compatible with GS even when done with a brute force analysis.

SUMMARY AND CONCLUSIONS

The critical exponents of the SF-BG transition in three dimensions have been determined by our extensive numerical simulations on the quantum hard-core DBH model and the classical J-current model. Our study reveals that the previously reported result $\phi \approx 1.1(1)$ is an artifact of fitting the data outside the quantum critical region. While the quantum critical region is hard to reach by tunning chemical potentials, the alternative strategy of tunning the disorder strength proves to provide us with a broader, accessible quantum critical region. Our simulation results, $\phi = 2.7(2), z = 3$ and $\nu = 0.88(5)$, are in perfect agreement with the scaling relation, $\phi = \nu z = \nu d$, proposed by Fisher *et al.*, thus resolving the ϕ-exponent "crisis".

In one dimension, we have carried out systematic analytical and numerical studies of the SF-BG transition. After the asymptotically exact RG theory of 1D SF-I transition is presented, we applied this theory to investigate the crossover behavior between the GS criticality and the weak-link criticality. With our analytical description on the crossover behavior, the interesting fact that the weak-link criticality dominates over the GS criticality at the multicritical point is revealed, leading to a smooth (parabolic) crossover behavior. On the numerical side, we verified the crucial assumption of the power-law scaling of the strength of the typical weakest weak link in the asymptotically exact RG theory. The GS transition line and a part the weak-link transition line are established. With the $\zeta = 2/3$ line, the multicritical point is also determined.

Although we have been focusing on the effect of disorder in chemical potential (diagonal disorder), our results, in general, applies also to the off-diagonal disorder case (disorder in

hopping amplitude and on-site interaction): for off-diagonal disorder, the critical behavior of the SF-I transition only becomes different with exact microscopic particle-hole symmetry where a new gapless, incompressible insulator, known as the Mott glass, emerges [63].

Although our study of the sXY criticality is limited to QPTs in 1D disordered boson systems, this criticality also applies to the SF-NL phase transitions of the XY model with strong parallel scratches. However, the superfluid response is anisotropic: the sXY criticality only applies to the direction perpendicular to the scratches; parallel to the scratches, the critical behavior of the superfluid response is expected to be described by the BKT physics (there is no instanton phase in the classical model). Another interesting problem worth exploring concerns the nature of the disorder-induced superfluidity. For the DBH models in one, two and three dimensions at unit filling, numeric simulations have shown that weak disorder always enhance superfluidity [16, 73]. However, a physical explanation of this observation (except in one dimension [46]) is still lacking.

BIBLIOGRAPHY

[1] B. Svistunov, E. Babaev, and N. Prokof'ev, Superfluid States of Matter (CRC Press, 2014).

[2] S. Sachdev, Quantum Phase Transitions (Cambridge University Press, 2011).

[3] S. L. Sondhi, S. M. Girvin, J. P. Carini, D. Shahar, Continuous quantum phase transitions, Rev. Mod. Phys. **69**, 315–333 (1997).

[4] R. Yu *et al.*, Bose glass and Mott glass of quasiparticles in a doped quantum magnet, Nature. **489**, 379–384 (2012).

[5] R. Yu *et al.*, Quantum critical scaling at a Bose-glass/superfluid transition: Theory and experiment for a model quantum magnet, Phys. Rev. B. **86**, 134421 (2012).

[6] P. B. Weichman, R. Mukhopadhyay, Critical Dynamics of the Dirty Boson Problem: Revisiting the Equality $z = d$, Phys. Rev. Lett. **98**, 245701 (2007).

[7] M. P. A. Fisher, P. B. Weichman, G. Grinstein, D. S. Fisher, Boson localization and the superfluid-insulator transition, Phys. Rev. B. **40**, 546–570 (1989).

[8] M. White *et al.*, Strongly Interacting Bosons in a Disordered Optical Lattice, Phys. Rev. Lett. **102**, 055301 (2009).

[9] M. Pasienski, D. McKay, M. White, B. DeMarco, A disordered insulator in an optical lattice, Nature Physics. **6**, 677–680 (2010).

[10] C. Meldgin *et al.*, Probing the Bose glass-superfluid transition using quantum quenches of disorder, Nature Physics. **12**, 646–649 (2016).

[11] A. Zheludev, T. Roscilde, Dirty-boson physics with magnetic insulators, Comptes Rendus Physique. **14**, 740–756 (2013).

[12] A. B. Harris, Effect of random defects on the critical behaviour of Ising models, J. Phys. C: Solid State Phys. **7**, 1671–1692 (1974).

[13] H. A. Brooks, The "Harris criterion" lives on, J. Phys.: Condens. Matter. **28**, 421006 (2016).

[14] J. Chayes, L. Chayes, D. S. Fisher, T. Spencer, Finite-Size Scaling and Correlation Lengths for Disordered Systems, Phys. Rev. Lett. **57**, 2999–3002 (1986).

[15] L. Pollet, N. Prokof'ev, B. Svistunov, M. Troyer, Absence of a Direct Superfluid to Mott Insulator Transition in Disordered Bose Systems, Phys. Rev. Lett. **103**, 140402 (2009).

[16] V. Gurarie, L. Pollet, N. Prokof'ev, B. Svistunov, M. Troyer, Phase diagram of the disordered Bose-Hubbard model, Phys. Rev. B. **80**, 214519 (2009).

[17] J. K. Freericks, H. Monien, Strong-coupling expansions for the pure and disordered Bose-Hubbard model, Phys. Rev. B. **53**, 2691–2700 (1996).

[18] P. B. Weichman, Dirty bosons: twenty years later, Mod. Phys. Lett. **B**. 22, 2623–2647 (2008).

[19] R. B. Griffiths, Nonanalytic Behavior Above the Critical Point in a Random Ising Ferromagnet, Phys. Rev. Lett. **23**, 17–19 (1969).

[20] B. McCoy, Incompleteness of the Critical Exponent Description for Ferromagnetic Systems Containing Random Impurities, Phys. Rev. Lett. **23**, 383–386 (1969).

[21] L. Pollet, A review of Monte Carlo simulations for the Bose–Hubbard model with diagonal disorder, Comptes Rendus Physique. **14**, 712–724 (2013).

[22] A. Young, Slow Dynamics at Quantum Phase Transitions, Int. J. Mod. Phys. C. **10**, 1391–1397 (1999).

[23] M. E. Fisher, M. Barber, D. Jasnow, Helicity Modulus, Superfluidity, and Scaling in Isotropic Systems, Phys. Rev. A. **8**, 1111–1124 (1973).

[24] J. Cardy, Scaling and Renormalization in Statistical Physics (Cambridge University Press, 1996).

[25] N. Goldenfeld, Lectures on Phase Transitions and the Renormalization Group (Westview Press, 1992).

[26] D. Stauffer, M. Ferer, M. Wortis, Universality of Second-Order Phase Transitions: The Scale Factor for the Correlation Length, Phys. Rev. Lett. **29**, 345–349 (1972).

[27] A. Aharony, Two-scale-factor universality and the ϵ-expansion, Phys. Rev. B. **9**, 2107–2109 (1974).

[28] P. C. Hohenberg, A. Aharony, B. Halperin, E. D. Siggia, Two-scale-factor universality and the renormalization group, Phys. Rev. B. **13**, 2986–2996 (1976).

[29] J. J. Sakurai, Modern quantum mechanics; rev. ed, (Addison-Wesley, Reading, MA, 1994).

[30] R. P. Feynman, A. R. Hibbs, Quantum mechanics and path integrals (McGraw-Hill, New York, NY, 1965).

[31] E. L. Pollock, D. M. Ceperley, Path-integral computation of superfluid densities, Phys. Rev. B. **36**, 8343–8352 (1987).

[32] N. Prokof'ev, B. Svistunov, I. S. Tupitsyn, "Worm" algorithm in quantum Monte Carlo simulations, Physics Letters A. **238**, 253–257 (1998).

[33] N. Prokof'ev, B. Svistunov, I. S. Tupitsyn, Exact, complete, and universal continuous-time worldline Monte Carlo approach to the statistics of discrete quantum systems, Sov. Phys. JETP **87**, 310–321 (1998).

[34] N. Prokof'ev, B. Svistunov, Worm Algorithm for Problems of Quantum and Classical Statistics, in: *Understanding Quantum Phase Transitions* (CRC Press, 2010), pp. 499–522.

[35] M. Girardeau, Relationship between Systems of Impenetrable Bosons and Fermions in One Dimension, J. Math. Phys. **1**, 516 (1960).

[36] F. D. M. Haldane, "Luttinger liquid theory" of one-dimensional quantum fluids. I. Properties of the Luttinger model and their extension to the general 1D interacting spinless Fermi gas, J. Phys. C: Solid State Phys. **14**, 2585–2609 (1981).

[37] F. D. M. Haldane, Effective Harmonic-Fluid Approach to Low-Energy Properties of One-Dimensional Quantum Fluids, Phys. Rev. Lett. **47**, 1840–1843 (1981).

[38] T. Giamarchi, Quantum physics in one dimension (Clarendon, Oxford, 2004).

[39] M. A. Cazalilla, R. Citro, T. Giamarchi, E. Orignac, M. Rigol, One dimensional bosons: From condensed matter systems to ultracold gases, Rev. Mod. Phys. **83**, 1405–1466 (2011).

[40] T. Giamarchi, H. J. Schulz, Localization and Interaction in One-Dimensional Quantum Fluids, EPL. **3**, 1287–1293 (1987).

[41] T. Giamarchi, H. Schulz, Anderson localization and interactions in one-dimensional metals, Phys. Rev. B. **37**, 325–340 (1988).

[42] Z. Yao, K. P. C. da Costa, M. Kiselev, N. Prokof'ev, Critical Exponents of the Superfluid–Bose-Glass Transition in Three Dimensions, Phys. Rev. Lett. **112**, 225301 (2014).

[43] C. Kane, M. P. A. Fisher, Transport in a one-channel Luttinger liquid, Phys. Rev. Lett. **68**, 1220–1223 (1992).

[44] C. Kane, M. P. A. Fisher, Transmission through barriers and resonant tunneling in an interacting one-dimensional electron gas, Phys. Rev. B. **46**, 15233–15262 (1992).

[45] A. Furusaki, N. Nagaosa, Single-barrier problem and Anderson localization in a one-dimensional interacting electron system, Phys. Rev. B. **47**, 4631–4643 (1993).

[46] B. Svistunov, Superfluid–Bose-glass transition in weakly disordered commensurate one-dimensional system, Phys. Rev. B. **54**, 16131–16134 (1996).

[47] V. A. Kashurnikov, A. I. Podlivaev, N. V. Prokof'ev, B. Svistunov, Supercurrent states in one-dimensional finite-size rings, Phys. Rev. B. **53**, 13091–13105 (1996).

[48] J. M. Kosterlitz, D. J. Thouless, Long range order and metastability in two dimensional solids and superfluids, J. Phys. C: Solid State Phys. **5**, L124–L126 (1972).

[49] J. M. Kosterlitz, D. J. Thouless, Ordering, metastability and phase transitions in two-dimensional systems, J. Phys. C: Solid State Phys. **6**, 1181–1203 (1973).

[50] J. M. Kosterlitz, The critical properties of the two-dimensional xy model, J. Phys. C: Solid State Phys. **7**, 1046–1060 (1974).

[51] E. Altman, Y. Kafri, A. Polkovnikov, G. Refael, Phase Transition in a System of One-Dimensional Bosons with Strong Disorder, Phys. Rev. Lett. **93**, 150402 (2004).

[52] E. Altman, Y. Kafri, A. Polkovnikov, G. Refael, Insulating Phases and Superfluid-Insulator Transition of Disordered Boson Chains, Phys. Rev. Lett. **100**, 170402 (2008).

[53] E. Altman, Y. Kafri, A. Polkovnikov, G. Refael, Superfluid-insulator transition of disordered bosons in one dimension, Phys. Rev. B. **81**, 174528 (2010).

[54] S. Pielawa, E. Altman, Numerical evidence for strong randomness scaling at a superfluid-insulator transition of one-dimensional bosons, Phys. Rev. B. **88**, 224201 (2013).

[55] G. Refael, E. Altman, Strong disorder renormalization group primer and the superfluid-insulator transition, Comptes Rendus Physique. **14**, 725–739 (2013).

[56] L. Pollet, N. Prokof'ev, B. Svistunov, Classical-field renormalization flow of one-dimensional disordered bosons, Phys. Rev. B. **87**, 144203 (2013).

[57] L. Pollet, N. Prokof'ev, B. Svistunov, Asymptotically exact scenario of strong-disorder criticality in one-dimensional superfluids, Phys. Rev. B. **89**, 054204 (2014).

[58] Z. Yao, L. Pollet, N. Prokof'ev, B. Svistunov, Superfluid-insulator transition in strongly disordered one-dimensional systems, New J. Phys. **18**, 045018 (2016).

[59] F. Hrahsheh, T. Vojta, Disordered Bosons in One Dimension: From Weak- to Strong-Randomness Criticality, Phys. Rev. Lett. **109**, 265303 (2012).

[60] W. Janke, H. Kleinert, How good is the villain approximation?, Nuclear Physics B **270**, 135–153 (1986).

[61] M. Wallin, E. S. Sørensen, S. Girvin, A. Young, Superconductor-insulator transition in two-dimensional dirty boson systems, Phys. Rev. B. **49**, 12115–12139 (1994).

[62] T. D. Kühner, S. R. White, H. Monien, One-dimensional Bose-Hubbard model with nearest-neighbor interaction, Phys. Rev. B. **61**, 12474–12489 (2000).

[63] T. Giamarchi, P. Le Doussal, E. Orignac, Competition of random and periodic potentials in interacting fermionic systems and classical equivalents: The Mott glass, Phys. Rev. B. **64**, 245119 (2001).

[64] N. Prokof'ev, B. Svistunov, Superfluid-Insulator Transition in Commensurate Disordered Bosonic Systems: Large-Scale Worm Algorithm Simulations, Phys. Rev. Lett. **92**, 015703 (2004).

[65] F. Alet, E. S. Sørensen, Cluster Monte Carlo algorithm for the quantum rotor model, Phys. Rev. E. **67**, 015701 (2003).

[66] S. Coleman, Aspects of Symmetry (Cambridge University Press, 1988).

[67] N. Nagaosa, Quantum Field Theory in Condensed Matter Physics (Springer Science & Business Media, 1999).

[68] S. Alexander, J. Bernasconi, W. Schneider, R. Orbach, Excitation dynamics in random one-dimensional systems, Rev. Mod. Phys. **53**, 175–198 (1981).

[69] N. V. Prokof'ev, B. Svistunov, Two definitions of superfluid density, Phys. Rev. B. **61**, 11282–11284 (2000).

[70] M. Gerster *et al.*, Superfluid density and quasi-long-range order in the one-dimensional disordered Bose-Hubbard model, New J. Phys. **18**, 015015 (2016).

[71] P. Hitchcock, E. S. Sørensen, Bose-glass to superfluid transition in the three-dimensional Bose-Hubbard model, Phys. Rev. B. **73**, 174523 (2006).

[72] N. Prokof'ev, B. Svistunov, Worm Algorithms for Classical Statistical Models, Phys. Rev. Lett. **87**, 160601 (2001).

[73] Ş. G. Söyler, M. Kiselev, N.V. Prokof'ev, and B.V. Svistunov, Phase diagram of the commensurate two-dimensional disordered Bose-Hubbard model, Phys. Rev. Lett. **107**, 185301 (2011).